Genome-wide CRISPR-Cas9 screen reveals the importance of the heparane sulphate pathway and the conserved oligomeric golgi complex for synthetic dsRNA uptake and Sindbis virus infection

Olivier Petitjean[1,*], Erika Girardi[1,*], Richard Patryk Ngondo[2], Vladimir Lupashin[3], Sébastien Pfeffer[1,‡]

1 Université de Strasbourg, Architecture et Réactivité de l'ARN, Institut de biologie moléculaire et cellulaire du CNRS, 2 allée Konrad Roentgen, 67084 Strasbourg France

2 Université de Strasbourg, Institut de Biologie Moléculaire des Plantes du CNRS, 12 rue du Général Zimmer, 67084 Strasbourg France

3 University of Arkansas for Medical Sciences, 4301 West Markham Street, Little Rock, Arkansas 72205, United States of America

* These authors contributed equally

‡ To whom correspondence should be addressed: spfeffer@unistra.fr

Abstract

Double stranded RNA (dsRNA) is the hallmark of many viral infections. dsRNA is produced either by RNA viruses during replication or by DNA viruses upon convergent transcription. Synthetic dsRNA is also able to mimic viral-induced activation of innate immune response and cell death. In this study, we employed a genome-wide CRISPR-Cas9 loss of function screen based on cell survival in order to identify genes implicated in the host response to dsRNA. By challenging HCT116 human cells with either synthetic dsRNA or Sindbis virus (SINV), we identified the heparan sulfate (HS) pathway as a crucial factor for dsRNA entry and we validated SINV dependency on HS. Interestingly, we uncovered a novel role for COG4, a component of the Conserved Oligomeric Golgi (COG) complex, as a factor involved in cell survival to both dsRNA and SINV in human cells. We showed that COG4 knock-out led to a decrease of extracellular HS, specifically affected dsRNA transfection efficiency and reduced viral production, explaining the increased cell survival of these mutants.

Importance

When facing a viral infection, the organism has to put in place a number of defense mechanisms in order to clear the pathogen from the cell. At the early phase of this preparation for fighting against the invader, the innate immune response is triggered by the sensing of danger signals. Among those molecular cues, double-stranded (dsRNA) is a very potent inducer of different reactions at the cellular level that can ultimately lead to cell death. Using a genome-wide screening approach, we set to identify genes involved in dsRNA entry, sensing and apoptosis induction in human cells. This allowed us to determine that the heparan sulfate pathway and the Conserved Oligomeric Golgi complex are key determinants allowing entry of both dsRNA and viral nucleic acid leading to cell death.

47 **Introduction**

48 Upon infection by a virus, numerous mechanisms are put in place at the cellular level to raise
49 the alarm and get rid of, or at least limit, the invader. One of the first barrier that the virus has
50 to overcome to is to enter the cell by taking advantage of wide diversity of ubiquitous or cell-
51 specific cellular receptors. In addition to protein receptors, glycosaminoglycans present at the
52 cell surface also represent crucial factors for efficient viral attachment and entry (1).
53 Glycosaminoglycans, and more precisely heparan sulfates are ubiquitously expressed in human
54 cells. They possess a global negative charge that is able to interact electrostatically with the
55 basic residues that are exposed by viral surface glycoproteins. This allows viruses to increase
56 their concentration at cell surface and so the possibility to interact with their specific entry
57 receptor (2). For instance, alphaviruses such as Semliki Forest virus (SFV) and Sindbis virus
58 (SINV) are enveloped positive-strand RNA viruses that contain two glycoproteins at the
59 envelope, the proteins E1 and E2. E2 is involved in the interaction of the virus particle to the
60 cell surface (3, 4), while E1 serves in the fusion process (5).

61 Once inside the cell, the replication of the viral genome represents another critical step to trigger
62 the antiviral immune response. Double-stranded (ds) RNA is a ubiquitous pathogen-associated
63 molecular pattern (PAMP) recognized by the cellular machinery, which can arise as a
64 replication intermediate for viruses with an RNA genome, or from convergent transcription for
65 DNA viruses (6). In mammals, dsRNA recognition is driven by specific receptors including the
66 cytoplasmic RIG-Like Receptors (RLRs) and endosomal Toll Like Receptors (TLRs) (7).
67 Sensing of dsRNA by these receptors results in the activation of a complex signaling cascade
68 leading to the production of type I interferon (IFN), which in turn triggers the expression of
69 IFN stimulated genes (ISG) and the establishment of the antiviral state (8). The ultimate
70 outcome of this vertebrate-specific antiviral response is translation arrest and cell death by
71 apoptosis (9).

72 The revolution brought by the discovery of the CRISPR-Cas9 technology has provided
73 biologists with an invaluable tool to edit the genome at will and easily perform individual gene
74 knock-out (10). This technique is perfectly suited to perform genome-wide screens in a
75 relatively fast and easy to implement manner, especially when the readout is based on cell
76 survival. For this reason, numerous CRISPR-Cas9 loss of function screens have been performed
77 based on cell survival after infection with different viruses (11–13). These approaches allowed
78 the identification of novel virus specific as well as common factors involved in antiviral defense
79 mechanisms or in cellular permissivity to virus infection.
80 Here, we chose to take advantage of the fact that dsRNA is almost always detected in virus-
81 infected cells (6) and is a potent inducer of apoptosis to design a genome-wide screen aiming
82 at identifying host genes that when edited resulted in increased cell survival to dsRNA and viral
83 challenge. To this aim, we performed a CRISPR-Cas9 screen based on cell survival in HCT116
84 cells after either cationic lipid-based transfection of an *in vitro* transcribed long dsRNA or
85 infection with the model alphavirus SINV, which replicates *via* a dsRNA intermediate.
86 Our results indicate that genes involved in limiting attachment and therefore entry, be it of the
87 synthetic dsRNA or SINV, are vastly over-represented after selection. We validated two genes
88 of the heparan sulfate pathway (namely *SLC35B2* and *B4GALT7*) as required for dsRNA
89 transfectability and SINV infectivity. We also identified and characterized COG4, a component
90 of the Conserved Oligomeric Golgi (COG) complex, as a novel factor involved in susceptibility
91 to dsRNA and viral induced cell death linked to the heparan sulfate biogenesis pathway.
92
93 **Results**
94 **Genome-wide CRISPR/Cas9 screen based on cell survival upon dsRNA transfection**
95 **identify factors of the heparan sulfate pathway**
96 In order to identify cellular genes that are involved in the cellular response to dsRNA which
97 culminates with cell death, we performed a CRISPR/Cas9 genome-wide loss-of-function screen

98 in the human colon carcinoma cell line HCT116. This cell line is highly suitable for
99 CRISPR/Cas9 genetic screening procedures (14) and can be easily infected with SINV with
100 visible cytopathic effects at 24 and 48 hours post infection (hpi) (Fig. S1A). Moreover,
101 transfection of an *in vitro* transcribed 231 bp-long dsRNA by a cationic lipid-based transfection
102 reagent in HCT116 cells led to strong cell death at 24 and 48 hours post treatment (hpt) (Fig.
103 S1B).
104 We generated a Cas9-expressing HCT116 monoclonal cell line (Fig. S1C) that we stably
105 transduced with the human genome-wide lentiviral Brunello library composed of 76 441
106 sgRNAs targeting 19 114 genes, as well as about 1000 non-targeting sgRNAs as controls (15).
107 We then applied a positive selection by lipofecting 30 million transduced cells per replicate
108 with the synthetic long dsRNA and we collected the surviving cells 48h later. In parallel, the
109 same initial amount of stably transduced cells was left untreated as control for (Input) for each
110 replicate (Fig. 1A). DNA libraries from the input samples were generated, sequenced and
111 quality checked. In particular, we verified the sgRNA coverage by observing the presence of
112 the 4 guides per genes for 18 960 genes (99.2% of the genes) and 3 sgRNAs per gene for the
113 remaining 154 genes (0.2% of the genes) (Dataset S1).
114 Using the MAGeCK software (16), we assessed the normalized read count distribution of the
115 control and dsRNA-treated biological triplicates, which, despite a quite homogenous sgRNA
116 distribution, showed the presence of few outliers upon selection (Fig. 1B). We identified eight
117 genes that were significantly enriched with a false discovery rate lower than 1% (FDR1%).
118 Among those, four genes belonged to the heparan sulphate biosynthesis pathway (namely,
119 *SLC35B2*, *B4GALT7*, *EXT1* and *EXT2*) and three were components of the conserved oligomeric
120 golgi complex (namely *COG3*, *COG4* and *COG8*) (Fig. 1C, Dataset S2). In particular, all four
121 sgRNAs targeting each of *SLC35B2*, *B4GALT7, COG4* genes were enriched upon dsRNA
122 selection (Fig. S1D).

123 Heparan sulphate (HS) is a linear polysaccharide that is covalently attached to core proteins in
124 proteoglycans (PG) on the cell surface (for review, see Li and Kusche-Gullberg, 2016). Among
125 many properties, HS play a role in binding of protein ligands and as a carrier for lipases,
126 chemokines and growth factor (Bishop et al., 2007; Li and Kusche-Gullberg, 2016), but also as
127 a viral receptor (19). HS biosynthesis takes place in the Golgi, where most of the biosynthetic
128 enzymes are anchored to the Golgi membrane (20).
129 We first validated the resistance phenotype to dsRNA of *SLC35B2* and *B4GALT7*, the two top
130 hits identified in the screen (Fig. 1C, Fig. S1D), by generating two individual knock-out clones
131 for each gene by CRISPR-Cas9 editing in HCT116cas9 (Fig. S2). Knock-out of either *SLC35B2*
132 or *B4GALT7* genes abolished cell death induced by dsRNA lipofection compared to parental
133 HCT116cas9 cells, as assessed by the measurement of cell viability 48h post transfection (Fig.
134 1D, left part of the graph). These results demonstrated the involvement of SLC35B2 and
135 B4GALT7 in dsRNA-induced cell death.
136 The observed resistance to dsRNA in the mutants could occur at many different steps: dsRNA
137 liposome attachment and entry, recognition, induction of the IFN pathway or apoptosis. To test
138 whether the first step was affected, we employed a nucleic acid delivery method that was not
139 based on cationic lipid transfection. In particular, we used nucleofection (an electroporation-
140 based transfection method) to introduce long dsRNAs into HCT116 cells and we showed that
141 this approach totally restored cell death in *SLC35B2* and *B4GALT7* knock-out cells (Fig. 1D,
142 right part of the graph). In addition, we also performed liposome-based transfection of an *in*
143 *vitro* transcribed Cy5-labelled dsRNA in *SLC35B2* and *B4GALT7* KO cells and assessed the
144 Cy5 fluorescence at 48 h post-transfection by FACS analysis (Fig. 1E-F). Although the number
145 of Cy5 positives (Cy5+) cells was not significantly different in the *B4GALT7* KO clones and
146 only slightly lower in the *SLC35B2* KO cells compared to WT cells (Fig. 1E), we observed a
147 significant reduction of at least 80% of the median Cy5 fluoresence in both *B4GALT7* and

148 *SLC35B2* KO cells relative to control (Fig. 1F), thereby indicating a significant drop in the
149 number of transfected Cy5-labeled RNA molecules per cells.
150 We also confirmed that liposome-based transfection of nucleic acid such as plasmidic DNA
151 was impaired in *SLC35B2* and *B4GALT7* KO cells, by transfecting a GFP-expressing plasmid
152 using Lipofectamine 2000 in wild type or knock-out cells (Fig. S3A, left panels and Fig. S3B).
153 Nonetheless, GFP expression could be restored in all cell lines upon nucleofection (Fig. S3A,
154 right panels).
155 To establish whether impairment of the HS synthesis is directly linked to a defect in dsRNA
156 entry and increased cell survival, we measured the extracellular HS levels in *SLC35B2* and
157 *B4GALT7* KO cells. We measured a substantial reduction of the extracellular HS staining as
158 assessed by FACS measurement of two independent *SLC35B2* and *B4GALT7* KO clones
159 compared to HCT116 wild type cells (Fig. 1G). To confirm the importance of HS at the cell
160 surface for liposome-based transfection, we mimicked the HS-defective phenotype by
161 removing extracellular HS in parental HCT116cas9 cells either enzymatically (with heparinase)
162 or chemically (with sodium chlorate NaClO3) (Fig. S3C-D). We tested the transfectability of a
163 GFP-expressing plasmid by measuring either the relative number of GFP positive cells or the
164 relative median of GFP intensity of fluorescence by FACS analysis. Although the relative
165 number of GFP positive cells was not significantly reduced by heparinase treatment (Fig. S3C),
166 it caused a reduction in GFP intensity in HCT116cas9 treated cells, thereby recapitulating the
167 GFP plasmid lipofection defect observed in *SLC35B2* and *B4GALT7* KO (Fig. S3D). Moreover,
168 this effect correlates with the reduction of extracellular HS by enzymatic treatment quantified
169 by FACS (Fig. S3E), which demonstrates that extracellular HS are crucial for transfection by
170 lipofection. In the case of NaClO3 treatment, despite the reduction in both the relative number
171 of GFP positive cells (Fig. S3C) and the relative median of GFP intensity of fluorescence(Fig.
172 S3D) compared to control, we could not observe a correlation with a decrease in overall

173 extracellular HS (Fig. S3E). This could be due to the fact that while a mix of heparinase I & III
174 remove every kind of extracellular heparan sulfates, NaClO3 only impairs the O-sulfation (21).
175 Taken together, our results show that knocking out *SLC35B2* and *B4GALT7* results in reduced
176 levels of extracellular HS, which in turn impairs liposome-based transfectability of HCT116
177 cells. Moreover, the validation of these two top hits indicates that other candidates might be
178 suitable for further analysis and may also have an impact on the dsRNA resistance phenotype.
179

180 **COG4 is involved in dsRNA-induced cell death partly via the heparan sulphate pathway**

181 Among the significant hits of our genome-wide screen were proteins related to COG complex,
182 namely COG4, COG3 and COG8. The COG complex is a hetero-octameric complex containing
183 8 subunits (COG1-8) interacting with numerous proteins mainly involved in intra-Golgi
184 membrane trafficking such as vesicular coats, Rab proteins and proteins involved in SNARE
185 complex (22, 23). This interaction with the trafficking machinery is crucial for the proper
186 functionality of the Golgi apparatus and mutations in the COG complex result in severe cellular
187 problems such as glycosylation defect (24–27), which are due to mislocalization of recycling
188 Golgi enzymes (28, 29).
189 Since we retrieved three out of the eight COG family members in our CRISPR/Cas9 screen
190 suggesting their importance in dsRNA-induced cell death, we tested the effect of their
191 inactivation by CRISPR-Cas9. *COG4* being the most enriched COG gene in our screen, we
192 generated a polyclonal *COG4* KO HCT116cas9 cell line and validated their dsRNA resistance
193 phenotype resulting in an increase survival in response to synthetic dsRNA transfection (Fig.
194 S4A). We also observed a reduction in the relative number of Cy5 positives (Cy5+) cells and
195 the median Cy5 fluorescence in *COG4* KO cells relative to control by FACS analysis (Fig.
196 S4B-C).

197 To further confirm the involvement of the COG complex, we also tested the effect of dsRNA
198 transfection in previously generated HEK293T KO *COG3*, 4 and 8 cells (Fig. 2A) (30).
199 Interestingly, while *COG8* mutants mutants did not display a significant survival phenotype in
200 response to dsRNA lipofection, *COG3* and *COG4* KO HEK293 cells did. In addition, the
201 survival phenotype could be complemented by stable expression of a COG4-GFP construct
202 compared to *COG4* KO cells (Fig. 2A). Moreover, although we could not detect a decrease in
203 the relative number of Cy5 positives (Cy5+) cells in *COG4* KO cells relative to the controls
204 (Fig. 2B), the median Cy5 fluorescence in *COG4* KO cells was significantly reduced compared
205 to both HEK293T and COG4 rescued cells (Fig. 2C), thereby indicating a significant decrease
206 in the number of transfected Cy5-labeled RNA molecules per cells.
207 In agreement, dsRNA accumulation appeared to be significantly reduced, but still present, in
208 HEK293T *COG4* KO cells compared to control cells as determined by RT-qPCR analysis of
209 dsRNA isolated from cells 24h after transfection (Fig 2D) and this correlated with reduced IFN-
210 beta accumulation in HEK293T KO *COG4* cells compared to control cells (Fig. 2E).
211 These results indicated that dsRNA transfectability was strongly reduced but not totally
212 impaired in the absence of COG4 and that dsRNA could be still detected in *COG4* KO cells in
213 order to activate type-I IFN response.
214 We confirmed the reduced internalization of dsRNAs in COG4 mutant cells by transfecting
215 rhodamine-labeled poly(I:C), a synthetic dsRNA analog, in HEK293T *COG4* KO or WT cells
216 (Fig. 2F) and by counting the number of poly I:C foci per cell at 6, 12 and 24 h post transfection
217 (Fig. 2G). We could observe a significant reduction in rhodamine positive foci in HEK293T
218 *COG4* KO during the time course, suggesting a defect in dsRNA internalization, which could
219 explain the increased survival phenotype.
220 In order to assess whether the *COG4* KO survival phenotype was associated with the heparan
221 sulphate pathway defect, we stained extracellular HS and measured the HS expression by FACS

222 analysis. We observed a decrease of extracellular HS in KO *COG4* cells compared to control
223 cells (WT and rescued), which demonstrated that the COG complex is related to the HS
224 biosynthesis pathway (Fig. S4D)
225 The reduction in extracellular HS could correlate with a decrease in transfectability and explain
226 the survival phenotype in KO *COG4* cells. Surprisingly however, lipofection of a GFP
227 expressing plasmid indicated that HEK293T *COG4* KO cells are still transfectable with a
228 plasmid DNA compared to control cells as observed by FACS analysis (Fig. S4E-F).
229 Altogether these findings indicate that the COG complex is involved in HS biosynthesis and
230 that removal of *COG4* results in a lower accumulation of HS at the cell surface, which most
231 likely translate in a reduced transfectability of dsRNA. However, as opposed to the observations
232 in *SLC35B2* or *B4GALT7* KO cells, the cells are still transfectable with a plasmid DNA and,
233 although to a lower extent, with dsRNA. Interestingly, the increased cell survival phenotype of
234 *COG4* KO cells upon dsRNA transfection does correlate with a reduced, but still measurable,
235 IFN-B production.
236

237 **Cell survival based genome-wide CRISPR/Cas9 screen identifies *COG4* as a permissivity**
238 **factor to SINV**

239 SINV is a small enveloped virus with a single stranded RNA genome of positive polarity. The
240 virus belongs to the *Togaviridae* family, alphavirus genus and is considered as the model for
241 other medically important viruses such as chikungunya virus (CHIKV) and Semliki forest virus
242 (SFV). During its infectious cycle, SINV produces dsRNA as a replication intermediate and
243 induces cytopathic effects in mammalian cells, leading to cell death within 24 to 48 h post-
244 infection (31).
245 In order to identify host genes that are related to SINV-induced cell death and infection, we
246 performed a CRISPR/Cas9 knock-out screen in HCT116cas9 cells, which are susceptible to

247 this virus (Fig. 3A, Fig. S1). After transduction with the CRISPR lentiviral genome-wide
248 knockout library, puromycin-resistant HCT116 cells were infected with SINV-GFP at a MOI
249 of 0.1 and selected for cell survival. Using the MAGeCK software (16), we assessed the
250 normalized read count distribution of the control and SINV-infected biological triplicates,
251 which, despite a quite homogenous sgRNA distribution, showed the presence of few outliers
252 upon selection (Fig. 3B). We identified two genes that were significantly enriched with a false
253 discovery rate lower than 25% (FDR25%), notably *SLC35B2* and *B4GALT7* (Dataset S3, Fig.
254 3C). Genes of the heparan sulphate pathway have been previously found in genome-wide
255 CRISPR-Cas9 loss of function studies looking for factors involved in the accumulation of
256 viruses such as Influenza, Zika and chikungunya virus (Han et al., 2018; Li et al., 2019; Tanaka
257 et al., 2017). Interestingly, among the top-ranking hits, we retrieved *COG4*, which was not
258 previously associated with SINV infection (Fig. 3C).
259 To validate the involvement of *COG4* during SINV infection, we infected HEK293T, *COG4*
260 KO or COG4 KO rescued HEK293T cells with SINV and measured cell viability at 24, 48 and
261 72 hpi. The cell viability assay revealed that the *COG4* KO cells were less sensitive at early
262 times points of SINV infection (24 & 48 hpi), but this tendency disappeared at 72 hpi (Fig. 3D.
263 In agreement, the determination of viral titer by plaque assay showed that *COG4* KO HEK293T
264 cells produced significantly less infectious viral particles than HEK293T or *COG4*-rescued
265 cells at 24 hpi but not at 48 hpi, underlining a possible delay in the infection and virus-induced
266 cell death (Fig. 3E). We also observed that GFP accumulated to lower levels in *COG4* KO than
267 in WT cells both at 24 and 48 h post-infection (hpi) (Fig. S5A). Finally, we noticed that the
268 reduced viral production in KO *COG4* cells was associated with a reduced accumulation of
269 viral dsRNA in the cytoplasm, when we infected WT or *COG4* KO cells with SINV-GFP and
270 performed immunostaining with the anti-dsRNA J2 antibody 24 hpi (Fig. S5B). Overall, our

271 results indicate that COG4 expression is needed for an efficient SINV infection and that its
272 absence can delay the infection thereby increasing cell survival in COG4 KO cells.
273
274 **Discussion**

275 Several CRISPR/Cas9 screens aiming at identifying factors required for infection by specific
276 viruses have been described in the literature, but to our knowledge, none has been designed to
277 look at the effect of the only common factor between all those viruses, *i.e*. dsRNA. Here, we
278 used the Brunello sgRNA lentiviral library to screen for genes involved in HCT116 cells
279 survival to synthetic dsRNA transfection and to SINV infection. This allowed us to identify
280 components of the heparan sulphate biosynthesis pathway and of the COG complex as critical
281 host factors in the cellular response to above mentioned challenges. It has been already reported
282 that cell-survival-based CRISPR screens for viral host factors are biased toward genes linked
283 to the initial steps of the infection, and even more so to viral entry (11, 35). Thus, in our case,
284 HS is a well-known factor required for SINV entry due to the virus adaptation to cell culture
285 (36). We also retrieved genes of the HS pathway in our dsRNA-based screen, and we confirmed
286 the importance of extracellular HS for dsRNA-induced toxicity. This is mostly due to a decrease
287 of transfectability of the cells when HS are missing, which is linked to the fact that the
288 polyplexes used for transfection are positively charged and can interact electrostatically with
289 glycosaminoglycans (37, 38). Our work also points out to the limitations of survival-based
290 CRISPR-Cas9 screens, *i.e*. the selection pressure is too strong to allow the identification of
291 genes intervening after the entry step, thereby making the screen less sensitive. New strategies
292 should be designed to overcome this problem, such as using fluorescent-based cell sorting in
293 order to be less stringent in the selection.

294 In addition to the HS pathway, we identified members of the COG complex, and more
295 specifically *COG4*, as factors involved in dsRNA transfection and SINV infection. Loss of
296 function COG4 mutant cells show a dsRNA-resistant phenotype as well as a reduction in

297 extracellular HS expression, similar to previously published reports for other COG proteins (34,
298 39). Surprisingly, even if the removal of COG4 expression results in a defect in the HS pathway,
299 we were still able to transfect the KO *COG4* cell line either with a plasmid encoding GFP or,
300 although to a lesser extent, dsRNA. In addition, the dsRNA molecules that are able to enter into
301 HEK293T KO *COG4* are still sufficient to induce the IFN-β mRNA production indicating that
302 the innate immune response is still functional in these mutant background. Nonetheless, cell
303 death induced by dsRNA appears to be lower in *COG4* KO cells, most likely due to a delay in
304 the infection.
305 Future work will be needed in order to assess whether this phenotype upon SINV infection is
306 only correlated with a defect in HS biogenesis in *COG4* mutants or to other function of COG4.
307 The fact that *COG4* KO cells seem to better survive to both synthetic dsRNA transfection and
308 viral infection opens several interesting perspectives. Indeed, since the COG complex is related
309 to glycosylation and membrane trafficking (25, 40–42), deficiency in one or more of its
310 components could potentially lead to a glycosylation and/or subcellular localization defect of
311 components of the innate immune response or of the apoptosis pathway, although this
312 possibility remains to be formally proven. The difference of transfectability of plasmid DNA
313 and dsRNA in *COG4* KO cells is also intriguing and could indicate that different kinds of
314 nucleic acids do not necessarily use the exact same routes to enter the cells upon liposome-
315 based transfection. Finally, there could be other defects linked to COG deficiencies(40, 43) that
316 could account for our observations and elucidating those will require further work. It is
317 particularly interesting that *COG3* and *COG4* knock-out cells display a dsRNA-induced cell
318 death resistance phenotype, while *COG8* mutants do not. This implies that only part of the COG
319 complex is involved in dsRNA uptake.
320 In conclusion, our work uncovered *COG4* as a new player in the HS production, which is
321 required for both SINV infection and dsRNA transfection. These results also highlight that

322 synthetic dsRNA is a powerful tool to identify novel key pathways of the cellular response to
323 RNA viruses.
324
325 **Materials and Methods**
326 **Cell culture and virus**
327 HCT116, HEK293T, HEK293T COG KOs, BHK21 and Vero R cells were maintained in
328 Dulbecco's Modified Eagle Medium (DMEM) 4.5 g/L glucose (Gibco, Thermo Fisher
329 Scientific Inc.) supplemented with 10% fetal bovine serum (FBS) (Takara) in a humidified
330 atmosphere of 5% CO_2 at 37°C. HEK293T *COG3*, *COG8* and *COG4* KO and *COG4* KO stably
331 rescued with COG4-GFP were described previously (44, 45). HCT116cas9 and HEK293T
332 COG4rescued were maintained in the same medium with addition of 10 μg/mL blasticidine.
333 HCT116 KO clones (*COG4*, *SLC35B2*#1 and #2, *B4GALT7*#1 and #2 were maintained in the
334 same medium with addition of 10 μg/mL blasticdine and 1 μg/mL puromycine.
335 SINV wild type (SINV) or expressing the green fluorescent protein (SINV-GFP) were produced
336 as previously decribed (46) in BHK21 cells. In the later, the promoter of SINV subgenomic
337 RNA was duplicated and inserted at the 3' extremity of the viral genome, the GFP sequence
338 was then inserted after this new promoter. Cells were infected with either SINV WT or SINV
339 GFP at a MOI of 10^{-1} and samples were harvested at 24 or 48 hours post-infection (hpi).
340
341 **Standard plaque assay**
342 10-fold dilutions of the viral supernatant were prepared. 50 μl aliquots were inoculated onto
343 Vero R cell monolayers in 96-well plates for 1 hour. Afterwards, the inoculum was removed
344 and cells were cultured in 2.5% carboxymethyl cellulose for 72 h at 37ºC in a humidified
345 atmosphere of 5% CO_2. Plaques were counted manually under the microscope. For plaque
346 visualization, the medium was removed, cells were fixed with 4% formaldehyde for 20 min and

347 stained with 1x crystal violet solution (2% crystal violet (Sigma-Aldrich), 20% ethanol, 4%
348 formaldehyde).
349
350 **J2 immunostaining**
351 HEK293T or KO *COG4* HEK293T cells were plated on millicell EZ slide (Millipore) and were
352 infected with SINV at an MOI of 0.1 for 24h. Cells were fixed with 4% formaldehyde diluted
353 in PBS 1x for 10 min at room temperature, followed by incubation in blocking buffer (0.2%
354 Tween X-100; PBS 1x; 5% normal goat serum) for 1 h. J2 antibody (Scicons) diluted in
355 blocking buffer at 1:1000 was incubated over night at 4°C. Between each steps, cells were
356 washed with PBS 1X-Tween 0.2%. Secondary antibody goat anti-mouse Alexa 594
357 (ThermoFisher) diluted at 1:1000 in PBS 1x-Tween 0.2% were incubated for 1 h at room
358 temperature. After DAPI staining (1:5000 dilution in PBS 1x for 5 min), slides were mounted
359 with a coverslip over anti-fading medium and observed by epifluorescence microscopy using
360 the BX51 (Olympus) microscope with a X 40 objective.
361
362 **Generation of HCT116cas9 line**
363 The HCT116cas9 cells, expressing human codon-optimized S. pyogenes Cas9 protein, were
364 obtained by transducing wild type HCT116 colorectal carcinoma cell line (ATCC® CCL-
365 247™) with lentiCas9-Blast lentiviral vector (Addgene #52962). Briefly, wild-type HCT116
366 cells were cultured in standard DMEM (GIBCO) medium supplemented with 10% Fetal bovine
367 serum (FBS, Gibco) and 100 U/mL of penicillin-Streptomycin (Gibco) at 37°C in 5% CO_2. The
368 cells were transduced at 80% confluency in a 10 cm tissue culture plate, using 6 mL lentiviral
369 supernatant supplemented with 4μg/mL of polybrene (H9268, sigma) for 6 hours. The
370 transduction medium was replaced with fresh growing medium for 24h before starting the

371 selection. Transduced HCT116cas9 cells were selected for 10 days and maintained in growing
372 medium supplemented with 10μL/mL of Blasticidin (Invivogen).
373
374 **High titer lentiviral sgRNA library production**
375 The production of high titer Human sgRNA Brunello lentiviral library which contains 4 sgRNA
376 per gene (Doench et al 2018) (Addgene #73178), was performed by transfecting HEK293T
377 cells in five 15 cm tissue culture plates using PEI (Polyethylenimin Linear, MW 25,000, 23966-
378 1-A, Polysciences) transfection method (Boussif et al 1995). Briefly, for each 15 cm plate
379 containing 20 mL of medium, 10μg of sgRNA library, 8μg of psPAX2 and 2μg of pVSV diluted
380 in 500μL of NaCl 150 mM were combined with 40μL of PEI (1.25 mg/mL) dissolved in 500μL
381 of NaCl 150 mM. The mix was incubated 30 minutes at room temperature and the formed
382 complexes were added dropwise on the cells. After 6 hours, the medium was replaced and the
383 viral supernatant was collected after 48 hours and after 72 hours. The supernatant was filtered
384 through a 0.45μm PES filter and the viral particles concentrated 100 times using Lenti-X™
385 Concentrator (Takara) before storage at -80. The viral titer was established by counting
386 puromycin resistant colonies formed after transducing HCT116 cells with serial dilutions of
387 viral stock. HCT116cas9 cells were transduced with lentivirus-packaged Brunello sgRNA
388 library at a MOI of 0.3. The lentiviral library has been sequenced to verify that all the lenti-
389 sgRNA are represented.
390
391 **Genome-wide CRISPR/Cas9 knock-out screens**
392 For each replicate (n=3), 5x10^6 stably transduced cells/dish were seeded in 6x15cm^2 plate in
393 order to keep a 300X representativity of the sgRNA library. Untreated samples (Input) were
394 collected as controls. One day later, cells were either lipofected with 1 μg/mL dsRNA-Citrine
395 or infected with SINV at MOI of 0.1 and cultured at 37°C 5% CO_2. Cells were washed with

396 PBS 1X 48 hours post treatment, to remove dead cells and fresh media was added to surviving
397 clones. Cells were expanded and all cells were collected 6 days post dsRNA transfection and
398 18 days post SINV infection.
399 Genomic DNA was isolated by resuspending the cell pellet in 5 mL of resuspension buffer (50
400 mM Tris-HCl pH 8.0, 10 mM EDTA, 100 µg/ml RNaseA), 0,25 mL of 10% SDS was added
401 and incubated 10 mins at RT after mix. After incubation, the sample was sonicated and
402 incubated 30 mins at RT with 10 uL of proteinase K (10mg/mL). 5 mL of
403 Phenol/Chloroform/Isoamyl Alcohol solution was added and followed by a spin down 60 mins
404 at 12000g/20°C. Upper phase was transferred into a new tube and 500uL of NaAc 3M and 5
405 mL of isopropanol was added then incubation over night at RT and followed by a centrifuge 30
406 mins/20°C/12000g. Pellet was washed using EtOH and dissolve in H2O.
407 Illumina P5 and P7-barcoded adaptors were added by PCR on gDNA samples according to the
408 GoTaq protocol (Promega). PCR amplicons were gel purified and sequenced on a HiSeq4000
409 (Illumina) to obtain about 30 million reads for each samples. Enrichment of sgRNAs was
410 analysed using MaGeCK with default parameters (16). Primers used to generate the PCR
411 products are listed in Table S1. The results of the dsRNA and SINV screen are available in
412 Dataset S1 and S2, respectively
413
414 **Generation of monoclonal SLC35B2 and B4GALT7 and polyclonal COG4 knock-out**
415 **HCT116 cell lines**
416 The sgRNA expression vectors targeting either SLC35B2,B4GALT7 or COG4 (sgRNA
417 sequences selected were the 2 most enriched sgRNA from the Brunello library in the dsRNA
418 screen) genes were produced by annealing the "sense" and "antisense" oligonucleotides (Table
419 S1) at a concentration of 10 µM in 10 mM Tris-HCl (pH 8.0), 50 mM MgCl2 in 100 μL. The
420 mixture was incubated at 95 ° C for 5 minutes and then allowed to cool down to room

421 temperature. The oligonucleotide duplex thus formed was cloned into the BbsI restriction site
422 of the plasmid pKLV-U6gRNA (BbsI)-pGKpuro2ABFP (Addgene#62348). The lentiviral
423 supernatant from single transfer vector was produced by transfecting HEK293T cells (ATCC®
424 CRL-3216™) with the transfer vector, psPAX2 packaging plasmid (Addgene #12260) and the
425 pVSV envelope plasmid (Addgene #8454) in proportion 5:4:1 using Lipofectamine™ 2000
426 (Themofisher) reagent according to manufacturer protocol. Standard DMEM (GIBCO) medium
427 supplemented with 10% Fetal bovine serum (FBS, Gibco) and 100 U/mL of penicillin-
428 Streptomycin (Gibco) was used for growing HEK293T cells and for lentivirus production. One
429 10 cm plate of HEK293T cells at 70-80% confluency was used for the transfection. The medium
430 was replaced 8 hours post-transfection. After 48 hours the medium containing viral particles
431 was collected and filtered through a 0.45μm PES filter. The supernatant was directly used for
432 transfection or stored at -80°C. A 6 well plate of HCT116cas9 cells at 80% confluency was
433 transduced using 600 μL of lentiviral supernatant (300 μL of each lentivirus produced for each
434 duplexes) supplemented with 4 μg/mL polybrene (Sigma) for 6 hours. The transduction media
435 was then changed with fresh DMEM for 24 hours then the transduced cells were selected using
436 DMEM containing 10 μg/mL Blasticidin (Invivogen) and 1 μg/mL Puromycin (Invivogen).
437 Genomic DNA was isolated from individual colonies and KO clones were screened by PCR
438 (primers in Table S1). The expected WT band for SLC35B2 is 469 bp and the mutant band 132
439 bp. For B4GALT7, the WT band is 341 bp and mutant band 180 bp. For laboratory purposes,
440 the SLC35B2 clones have been generated into HCT116cas9 cells that are expressing mCherry
441 and Citrine due to integration of miReporter-PGK (Addgene#82477).
442
443 **Nucleic acids delivery**
444 Transfection using lipofectamine2000 (InvitroGen – 11668019) were performed following
445 manufacturer's instructions. For nucleofection, cells were nucleofected using Nucleofector SE

446 solution and reagent into Nucleocuvette following manufacturer's instructions using 4D-
447 Nucleofector System (Lonza). The cell number and nucleic acid amounts are indicated in each
448 figure legends. P-EGFP-N1 (Addgene plasmid#2491) was used in transfection and
449 nucleofection experiments as a control.
450
451 **Viability assay**
452 PrestoBlue (PB) reagent (ThermoFisher – A13261) was used for viability assay according to
453 the manufacturer's protocol. After 24 to 48 hours post treatment (SINV, dsRNA
454 transfection/nucleofection), cells were incubated with PB reagent and cell viability was
455 assessed by measuring the fluorescence (excitation 570 nm; emission 590 nm) after 20 mins
456 incubation using SAFAS spectrofluorometer (Xenius XC).Cell viability was expressed as a
457 percentage relative to untreated cells.
458
459 **Heparinase & sodium chlorate treatment and heparan sulfate staining**
460 Heparinase: 1*10^6 cells were treated with 2U of Heparinase I and III blend from
461 *Flavobacterium heparinum* (Merck – H3917) for 1 h at 37°C 5% CO2 in DMEM and then cells
462 were reverse transfected with 2 µg of GFP using lipofectamine2000 (Invitrogen) in 6 well plate.
463 Sodium chlorate: HCT116cas9 cells grow in 50 mM sodium chlorate (Merck – 1.06420)
464 DMEM 10 % FBS for at least 48 h then 150 000 cells were reverse transfected with 500 ng of
465 GFP using lipofectamine 2000 (Invitrogen) in 24 well plate.
466 24 (heparinase) or 48 (sodium chlorate) hours post treatment, cells were detach using PBS
467 0.02% EDTA then heparan sulfate of the cells were stained using 1:30 of F58-10E4 as primary
468 antibody (AMSBIO, cat#370255-S) in PBS 3% BSA for 30 to 40 minutes on ice then washed
469 with PBS 1% FBS and incubated with 1:30 anti-mouse Alexa Fluor 594 (Thermo, A-11032) in

470 PBS 3% BSA, washed twice using PBS 1% FBS then and analysed at FACS using
471 FACSCalibur.
472
473 **dsRNA preparation**
474 PCR fragments corresponding to 231 nts of the Citrine coding sequence were amplified from
475 ES-FUCCI plasmid (Addgene plasmid#62451) using primers containing T7 promoter sequence
476 with 2 distinct PCR fragment allowing the positive-sense or negative-sense RNA. Primers used
477 to generate the PCR products are listed in Table S1. The PCR fragments were produced using
478 DyNAzyme EXT DNA Polymerase (F-505S - Thermo Scientific) and purified using Monarch
479 DNA extraction (T1020L - New England Biolab). In vitro transcription (IVT) with homemade
480 T7 RNA polymerase was performed for 4 hours at 37°C. To label the IVT RNA, 1/10th of Cy5-
481 CTP (Amersham CyDye Fluorescent Nucleotides Cy5-CTP, GE Healthcare Life sciences) was
482 included in the IVT reaction. IVT RNA was digested with DNase I (EN0525 - Thermo
483 Scientific) for 30 min at 37°C and IVT product was purified, unincorporated nucleotides
484 removed and size checked using UV shadow (8% acrylamide-urea gel) followed by phenol-
485 chloroform extraction the nanodrop quantification for each strand. We then mix an equal
486 quantity of positive-strand and negative-strand RNA, heat for 5' at 95°C followed by slow cool
487 down to RT. The integrity of dsRNA is then checked by RNases T1 (EN0541 - Thermo
488 Scientific) and V1 (AM2275, Ambion) digestion.
489
490 **Microscopy**
491 Imaging of cells treated with dsRNA/GFP plasmid was carried out on the Observer A1 (Zeiss)
492 microscope and analyzed using Fiji (47). Images of cells transfected with Poly(I:C) (LMW)
493 Rhodamine (tlrl-piwr – Invivogen)(1,8 μg/mL, 24h post plating of 76 000 cells) into Lab-Tek
494 on glass coverslip (155411- Thermo Scientific) were acquired using a 100x Plan Apochromat

495 oil immersion NA1.4 objective on a spinning disk system Axio Observer Z1 (Zeiss) every 20
496 minutes for 72 hours. All pictures were acquired under the same conditions (laser power and
497 amplification gain) then processed with Fiji. Images of cells infected with SINV stained with
498 J2 antibody were carried out on the BX51 (Olympus).
499
500 **FACS analysis**
501 The cells intended for analysis by flow cytometry are recovered mechanically (PBS 0,5 mM
502 EDTA) or using trypsin, washed in PBS and then suspended in PBS 1 % FBS. Each acquisition
503 includes at least 10,000 events and is performed on the FACScalibur (BD Bioscience) device.
504 The data produced is processed using FlowJo software (FlowJo LLC).
505
506 **RT-qPCR analysis**
507 Total RNA was isolated using TRIzol (Invitrogen - 15596026) following manufacturer's
508 instructions. 1 µg of RNA was reverse transcribed using SuperScript IV Vilo (Invitrogen –
509 11756050) according to manufacturer's instructions. Real-time PCR was performed using
510 SYBR Green (Applied Biosystem – 4309155) and primers listed in Table S1 at an annealing
511 temperature of 60°C on a CFX96 thermal cycler (Biorad). Generated data were analysed using
512 the CFX Manager Software (Biorad).
513
514 **Western blot analysis**
515 Proteins were extracted using RIPA lysis buffer. Proteins were quantified by the Bradford
516 method and 20 to 30 µg of total protein extract was loaded on 4-20% Mini-PROTEAN®
517 TGX™ Precast Gels (Biorad). After transfer onto nitrocellulose membrane, equal loading was
518 verified by Ponceau staining. Membranes were blocked in 5% milk and probed with the

519 following antibodies: anti-Flag M2 (SIGMA, #F1804) and anti-GAPDH (clone 6C5, BioRad #
520 MCA4739P). Detection was performed using Chemiluminescent Substrate (Thermo Fisher).
521
522 **Data availability**
523 The CRISPR-Cas9 screen sequencing data discussed in this manuscript has been deposited on
524 NCBI's Sequence Read Archive (SRA) and has been attributed the submission ID
525 SUB8109948. It can be accessed at the following URL:
526 http://www.ncbi.nlm.nih.gov/bioproject/662202 (release pending).
527
528 **Acknowledgments**
529 The authors would like to thank members of the Pfeffer laboratory for discussion, Delphine
530 Richer for technical help, Dr. Jean-Daniel Fauny for help with the spinning disk microscope
531 and Dr. Frédéric Gros for help with FACS analysis, Dr Carla Saleh for providing us the SINV
532 WT and GFP clones.
533 This work was funded by the European Research Council (ERC-CoG-647455 RegulRNA) and
534 was performed under the framework of the LABEX: ANR-10-LABX-0036_NETRNA, which
535 benefits from a funding from the state managed by the French National Research Agency as
536 part of the Investments for the future program. This work has also received funding from the
537 People Programme (Marie Curie Actions) of the European Union's Seventh Framework
538 Program (FP7/2007-2013) under REA grant agreement n° PCOFUND-GA-2013-609102,
539 through the PRESTIGE program coordinated by Campus France (to EG), and from the French
540 Minister for Higher Education, Research and Innovation (PhD contract to OP). VL was
541 supported by the National Institutes of Health (R01GM083144).
542
543 **Authors contribution**

544 SP and EG conceived the project. SP, EG and OP designed the work and analysed the results.
545 OP, EG, and RPN performed the experiments. EG and OP set up the CRISPR/Cas9 screens,
546 RPN generated the lentivirus library and the HCT16-Cas9 cell line. OP and RPN performed the
547 bioinformatics analysis of the screens. OP generated the SLC35B2 and B4GALT7 KO clones.
548 OP generated IVT dsRNA and perform validation of cell survival. EG produced SINV-GFP
549 viral stock, performed the infections and analysed viral titers. OP performed FACS analyses.
550 EG and OP performed the immunofluorescence assays. OP analysed the live-imaging
551 microscopy data. VL provided the COG KO cells and antibodies. OP, EG and SP wrote the
552 manuscript with input from the other authors. SP and EG coordinated the work. SP assured
553 funding. All authors reviewed the final manuscript.
554

555 **References**

556 1. Bomsel M, Alfsen A. 2003. Entry of viruses through the epithelial barrier: pathogenic
557 trickery. Nat Rev Mol Cell Biol 4:57–68.
558 2. Rusnati M, Vicenzi E, Donalisio M, Oreste P, Landolfo S, Lembo D. 2009. Sulfated K5
559 Escherichia coli polysaccharide derivatives: A novel class of candidate antiviral
560 microbicides. Pharmacology & Therapeutics 123:310–322.
561 3. Byrnes AP, Griffin DE. 1998. Binding of Sindbis Virus to Cell Surface Heparan Sulfate. J
562 VIROL 72:8.
563 4. Smith TJ, Cheng RH, Olson NH, Peterson P, Chase E, Kuhn RJ, Baker TS. 1995. Putative
564 receptor binding sites on alphaviruses as visualized by cryoelectron microscopy.
565 Proceedings of the National Academy of Sciences 92:10648–10652.
566 5. Wahlberg JM, Bron R, Wilschut J, Garoff H. 1992. Membrane fusion of Semliki Forest
567 virus involves homotrimers of the fusion protein. J Virol 66:7309–7318.
568 6. Weber F, Wagner V, Rasmussen SB, Hartmann R, Paludan SR. 2006. Double-Stranded
569 RNA Is Produced by Positive-Strand RNA Viruses and DNA Viruses but Not in Detectable
570 Amounts by Negative-Strand RNA Viruses. Journal of Virology 80:5059–5064.
571 7. Schlee M, Hartmann G. 2016. Discriminating self from non-self in nucleic acid sensing.
572 Nat Rev Immunol 16:566–580.
573 8. Stetson DB, Medzhitov R. 2006. Type I Interferons in Host Defense. Immunity 25:373–
574 381.
575 9. García MA, Meurs EF, Esteban M. 2007. The dsRNA protein kinase PKR: Virus and cell
576 control. Biochimie 89:799–811.
577 10. Shalem O, Sanjana NE, Zhang F. 2015. High-throughput functional genomics using
578 CRISPR-Cas9. Nat Rev Genet 16:299–311.
579 11. Han J, Perez JT, Chen C, Li Y, Benitez A, Kandasamy M, Lee Y, Andrade J, tenOever B,
580 Manicassamy B. 2018. Genome-wide CRISPR/Cas9 Screen Identifies Host Factors
581 Essential for Influenza Virus Replication. Cell Reports 23:596–607.
582 12. Park RJ, Wang T, Koundakjian D, Hultquist JF, Lamothe-Molina P, Monel B, Schumann
583 K, Yu H, Krupzcak KM, Garcia-Beltran W, Piechocka-Trocha A, Krogan NJ, Marson A,
584 Sabatini DM, Lander ES, Hacohen N, Walker BD. 2017. A genome-wide CRISPR screen
585 identifies a restricted set of HIV host dependency factors. Nat Genet 49:193–203.
586 13. Zhang R, Miner JJ, Gorman MJ, Rausch K, Ramage H, White JP, Zuiani A, Zhang P,
587 Fernandez E, Zhang Q, Dowd KA, Pierson TC, Cherry S, Diamond MS. 2016. A CRISPR

588 screen defines a signal peptide processing pathway required by flaviviruses. Nature
589 535:164–168.
590 14. Golden RJ, Chen B, Li T, Braun J, Manjunath H, Chen X, Wu J, Schmid V, Chang T-C,
591 Kopp F, Ramirez-Martinez A, Tagliabracci VS, Chen ZJ, Xie Y, Mendell JT. 2017. An
592 Argonaute phosphorylation cycle promotes microRNA-mediated silencing. Nature
593 542:197–202.
594 15. Doench JG, Fusi N, Sullender M, Hegde M, Vaimberg EW, Donovan KF, Smith I, Tothova
595 Z, Wilen C, Orchard R, Virgin HW, Listgarten J, Root DE. 2016. Optimized sgRNA design
596 to maximize activity and minimize off-target effects of CRISPR-Cas9. Nat Biotechnol
597 34:184–191.
598 16. Li W, Xu H, Xiao T, Cong L, Love MI, Zhang F, Irizarry RA, Liu JS, Brown M, Liu XS.
599 2014. MAGeCK enables robust identification of essential genes from genome-scale
600 CRISPR/Cas9 knockout screens. Genome Biol 15:554.
601 17. Li J-P, Kusche-Gullberg M. 2016. Heparan Sulfate: Biosynthesis, Structure, and Function,
602 p. 215–273. *In* International Review of Cell and Molecular Biology. Elsevier.
603 18. Bishop JR, Schuksz M, Esko JD. 2007. Heparan sulphate proteoglycans fine-tune
604 mammalian physiology. Nature 446:1030–1037.
605 19. Cagno V, Tseligka ED, Jones ST, Tapparel C. 2019. Heparan Sulfate Proteoglycans and
606 Viral Attachment: True Receptors or Adaptation Bias? Viruses 11.
607 20. Lindahl U, Couchman J, Kimata K, Esko JD. 2015. Proteoglycans and Sulfated
608 Glycosaminoglycans, p. . *In* Varki, A, Cummings, RD, Esko, JD, Stanley, P, Hart, GW,
609 Aebi, M, Darvill, AG, Kinoshita, T, Packer, NH, Prestegard, JH, Schnaar, RL, Seeberger,
610 PH (eds.), Essentials of Glycobiology, 3rd ed. Cold Spring Harbor Laboratory Press, Cold
611 Spring Harbor (NY).
612 21. Safaiyan F, Kolset SO, Prydz K, Gottfridsson E, Lindahl U, Salmivirta M. 1999. Selective
613 Effects of Sodium Chlorate Treatment on the Sulfation of Heparan Sulfate. J Biol Chem
614 274:36267–36273.
615 22. Blackburn JB, D'Souza Z, Lupashin VV. 2019. Maintaining order: COG complex controls
616 Golgi trafficking, processing, and sorting. FEBS Lett 593:2466–2487.
617 23. Willett R, Ungar D, Lupashin V. 2013. The Golgi puppet master: COG complex at center
618 stage of membrane trafficking interactions. Histochem Cell Biol 140:271–283.
619 24. Kranz C, Ng BG, Sun L, Sharma V, Eklund EA, Miura Y, Ungar D, Lupashin V, Winkel
620 RD, Cipollo JF, Costello CE, Loh E, Hong W, Freeze HH. 2007. COG8 deficiency causes
621 new congenital disorder of glycosylation type IIh. Human Molecular Genetics 16:731–741.

622 25. Reynders E, Foulquier F, Leão Teles E, Quelhas D, Morelle W, Rabouille C, Annaert W,
623 Matthijs G. 2009. Golgi function and dysfunction in the first COG4-deficient CDG type II
624 patient. Human Molecular Genetics 18:3244–3256.
625 26. Spaapen LJM, Bakker JA, van der Meer SB, Sijstermans HJ, Steet RA, Wevers RA, Jaeken
626 J. 2005. Clinical and biochemical presentation of siblings with COG-7 deficiency, a lethal
627 multiple O- and N-glycosylation disorder. J Inherit Metab Dis 28:707–714.
628 27. Zeevaert R, Foulquier F, Jaeken J, Matthijs G. 2008. Deficiencies in subunits of the
629 Conserved Oligomeric Golgi (COG) complex define a novel group of Congenital
630 Disorders of Glycosylation. Molecular Genetics and Metabolism 93:15–21.
631 28. Shestakova A, Zolov S, Lupashin V. 2006. COG Complex-Mediated Recycling of Golgi
632 Glycosyltransferases is Essential for Normal Protein Glycosylation: COG Complex and
633 Golgi Glycosylation. Traffic 7:191–204.
634 29. Zolov SN, Lupashin VV. 2005. Cog3p depletion blocks vesicle-mediated Golgi retrograde
635 trafficking in HeLa cells. J Cell Biol 168:747–759.
636 30. Bailey Blackburn J, Pokrovskaya I, Fisher P, Ungar D, Lupashin VV. 2016. COG Complex
637 Complexities: Detailed Characterization of a Complete Set of HEK293T Cells Lacking
638 Individual COG Subunits. Front Cell Dev Biol 4.
639 31. Strauss JH, Strauss EG. 1994. The alphaviruses: gene expression, replication, and
640 evolution. Microbiol Rev 58:491–562.
641 32. Li Y, Muffat J, Omer Javed A, Keys HR, Lungjangwa T, Bosch I, Khan M, Virgilio MC,
642 Gehrke L, Sabatini DM, Jaenisch R. 2019. Genome-wide CRISPR screen for Zika virus
643 resistance in human neural cells. Proc Natl Acad Sci USA 201900867.
644 33. Murakami S, Takenaka-Uema A, Kobayashi T, Kato K, Shimojima M, Palmarini M,
645 Horimoto T. 2017. Heparan Sulfate Proteoglycan Is an Important Attachment Factor for
646 Cell Entry of Akabane and Schmallenberg Viruses. J Virol 91:e00503-17,
647 /jvi/91/15/e00503-17.atom.
648 34. Tanaka A, Tumkosit U, Nakamura S, Motooka D, Kishishita N, Priengprom T, Sa-ngasang
649 A, Kinoshita T, Takeda N, Maeda Y. 2017. Genome-Wide Screening Uncovers the
650 Significance of N-Sulfation of Heparan Sulfate as a Host Cell Factor for Chikungunya
651 Virus Infection. J Virol 91:e00432-17, /jvi/91/13/e00432-17.atom.
652 35. Savidis G, McDougall WM, Meraner P, Perreira JM, Portmann JM, Trincucci G, John SP,
653 Aker AM, Renzette N, Robbins DR, Guo Z, Green S, Kowalik TF, Brass AL. 2016.
654 Identification of Zika Virus and Dengue Virus Dependency Factors using Functional
655 Genomics. Cell Reports 16:232–246.

656 36. Klimstra WB, Ryman KD, Johnston RE. 1998. Adaptation of Sindbis Virus to BHK Cells
657 Selects for Use of Heparan Sulfate as an Attachment Receptor. Journal of Virology
658 72:7357–7366.
659 37. Mislick KA, Baldeschwieler JD. 1996. Evidence for the role of proteoglycans in cation-
660 mediated gene transfer. Proceedings of the National Academy of Sciences 93:12349–
661 12354.
662 38. Payne CK, Jones SA, Chen C, Zhuang X. 2007. Internalization and Trafficking of Cell
663 Surface Proteoglycans and Proteoglycan-Binding Ligands. Traffic 8:389–401.
664 39. Jae LT, Raaben M, Riemersma M, van Beusekom E, Blomen VA, Velds A, Kerkhoven
665 RM, Carette JE, Topaloglu H, Meinecke P, Wessels MW, Lefeber DJ, Whelan SP, van
666 Bokhoven H, Brummelkamp TR. 2013. Deciphering the Glycosylome of
667 Dystroglycanopathies Using Haploid Screens for Lassa Virus Entry. Science 340:479–483.
668 40. Blackburn JB, Kudlyk T, Pokrovskaya I, Lupashin VV. 2018. More than just sugars:
669 Conserved oligomeric Golgi complex deficiency causes glycosylation-independent
670 cellular defects. Traffic 19:463–480.
671 41. Ungar D, Oka T, Brittle EE, Vasile E, Lupashin VV, Chatterton JE, Heuser JE, Krieger M,
672 Waters MG. 2002. Characterization of a mammalian Golgi-localized protein complex,
673 COG, that is required for normal Golgi morphology and function. The Journal of Cell
674 Biology 157:405–415.
675 42. Willett R, Ungar D, Lupashin V. 2013. The Golgi puppet master: COG complex at center
676 stage of membrane trafficking interactions. Histochem Cell Biol 140:271–283.
677 43. D'Souza Z, Blackburn JB, Kudlyk T, Pokrovskaya ID, Lupashin VV. 2019. Defects in
678 COG-Mediated Golgi Trafficking Alter Endo-Lysosomal System in Human Cells. Front
679 Cell Dev Biol 7:118.
680 44. Climer LK, Pokrovskaya ID, Blackburn JB, Lupashin VV. 2018. Membrane detachment
681 is not essential for COG complex function. MBoC 29:964–974.
682 45. Blackburn JB, Lupashin VV. 2016. Creating Knockouts of Conserved Oligomeric Golgi
683 Complex Subunits Using CRISPR-Mediated Gene Editing Paired with a Selection Strategy
684 Based on Glycosylation Defects Associated with Impaired COG Complex Function, p.
685 145–161. *In* Brown, WJ (ed.), The Golgi Complex. Springer New York, New York, NY.
686 46. López P, Girardi E, Mounce BC, Weiss A, Chane-Woon-Ming B, Messmer M, Kaukinen
687 P, Kopp A, Bortolamiol-Becet D, Fendri A, Vignuzzi M, Brino L, Pfeffer S. 2020. High-
688 throughput fluorescence-based screen identifies the neuronal microRNA miR-124 as a
689 positive regulator of alphavirus infection. J Virol JVI.02145-19, jvi;JVI.02145-19v1.

690 47. Schindelin J, Arganda-Carreras I, Frise E, Kaynig V, Longair M, Pietzsch T, Preibisch S,
691 Rueden C, Saalfeld S, Schmid B, Tinevez J-Y, White DJ, Hartenstein V, Eliceiri K,
692 Tomancak P, Cardona A. 2012. Fiji: an open-source platform for biological-image
693 analysis. Nat Methods 9:676–682.
694 48. Sievers F, Wilm A, Dineen D, Gibson TJ, Karplus K, Li W, Lopez R, McWilliam H,
695 Remmert M, Söding J, Thompson JD, Higgins DG. 2011. Fast, scalable generation of high-
696 quality protein multiple sequence alignments using Clustal Omega. Mol Syst Biol 7:539.
697

698 **Figures legends**

699 **Figure 1. CRISPR-Cas9 survival screen to long dsRNAs identifies the extracellular**
700 **heparan-sulfates as necessary for nucleic acids internalization and cell death induction.**
701 **A.** Schematic representation of the CRISPR-Cas9 approach. HCT116 cells stably expressing a
702 human codon-optimized *S. pyogenes* Cas9 protein were transduced with the lentiviral sgRNA
703 library Brunello (MOI 0.3). 60*10^6 cells transduced cells were selected with 1 μg/mL
704 puromycin to obtain a mutant cell population to cover at least 300X the library. Selective
705 pressure via synthetic long dsRNA (1 μg/mL) was applied to induce cell death (in red). DNA
706 libraries from input cells and cells surviving the dsRNA treatment as three independent
707 biological replicates were sequenced on an Illumina HiSeq4000. Comparison of the relative
708 sgRNA boundance in the Input and dsRNA condition were done using the MAGeCK standard
709 pipeline. **B.** Median normalized read count distribution of all sgRNAs for the Input (in black)
710 and dsRNA (in red) replicates**. C.** Bubble plot of the candidate genes. Significance of RRA
711 score was calculated for each gene in the dsRNA condition compared to INPUT using the
712 MAGeCK software. The number of enriched sgRNAs for each gene is represented by the
713 bubble size. The gene ontology pathways associated to the significant top hits are indicated in
714 orange and green. **D.** Viability assay. Cells were transfected (80 000 cells; 1 μg/mL) or
715 nucleofected (200 000 cells; 400 ng) with synthetic long dsRNA and cell viability was
716 quantified 24 h (nucleofection) or 48 h (transfection) post treatment using PrestoBlue reagent.
717 Average of at least three independent biological experiments +/- SD is shown. One-way
718 ANOVA analysis, * $p < 0.05$. **E-F.** Cy5-labeled dsRNA (80 000 cells; 1 μg/mL) was transfected
719 into HCT116cas9, B4GALT7#1 and 2, SLC35B2#1 and #2 cells and Cy5 fluorescence was
720 quantified using FACS (10 000 events). The relative number of the Cy5 positive (Cy5+) cells
721 (**E**) and the relative median of Cy5 intensity of fluorescence (**F**) compared to HCT116cas9 cells
722 are shown. Average of three independent biological experiments +/- SD are shown. Paired t.test

723 analysis, * $p < 0.05$. **G.** Quantification of extracellular heparan-sulfates. FACS analysis of
724 HCT116 control or KO clones stained with the HS-specific antibody 10E4 (in red) compared
725 to unstained samples (in blue) (10 000 events). One representative experiment out of three is
726 shown.
727
728 **Figure 2. *COG4* is a novel host susceptibility factor to long dsRNA induced cell death.**
729 **A.** Viability assay. Cells (80 000 cells; 1 µg/mL) were transfected with dsRNA then the
730 viability of the cells was quantified 48 h post transfection using PrestoBlue reagent. Data from
731 at least three independent biological experiments are shown. One-way ANOVA analysis, * $p <$
732 0.05. **B-C.**Cy5-labeled dsRNA transfection (80 000 cells; 1 µg/mL) in HEK293T, KO COG4
733 and rescued cells. Cy5 fluorescence was quantified using FACSCalibur (10 000 events). The
734 percentage of Cy5+ cells (**B**) and the relative median of Cy5 intensity of fluorescence (**C**)
735 compared to parental HEK293T cells is shown. Average of three experiments +/- SD are shown.
736 Paired t.test analysi analysis, * $p < 0.05$. **D-E.** qPCR quantification of dsRNA and IFN-beta.
737 Cells (300 000 cells; 1 µg/mL) were transfected with synthetic long dsRNA. Total RNA was
738 extracted 24 h post transfection and quantified by RT-qPCR. The histogram represents the
739 expression fold change of synthetic dsRNA (**D**) and IFN-B mRNA (**E**) relative to GAPDH
740 mRNA in dsRNA transfected HEK293T KO COG4 rescued compared to HEK293T KO
741 COG4. Average of three independent biological experiments +/- SD are shown. Paired t.test
742 analysis, * $p < 0.05$. **F-G.** poly I:C rhodamine transfection and immunofluorescence in
743 HEK293T and HEK293T KO COG4. Cells were transfected with rhodamine-labeled poly I:C
744 (in red) and with a Rab5-GFP plasmid (in green). Images were acquired using a spinning disk
745 microscope at different time post transfection. Representative pictures (**E**) and the
746 approximative number of rhodamine-positive foci per cells quantified by counting 7 fields per
747 conditions (**F**) are shown. Two-way ANOVA analysis, * $p < 0.05$.

748

749 **Figure 3. CRISPR-Cas9 screen identifies *COG4* as a permissivity factor to SINV**

750 **A.** Schematic representation of the CRISPR-Cas9 approach. HCT116 cells stably expressing a
751 human codon-optimized *S. pyogenes* Cas9 protein were transduced with the lentiviral sgRNA
752 library Brunello (MOI 0.3). 60*10^6 cells transduced cells were selected with 1 μg/mL
753 puromycin to obtain a mutant cell population to cover at least 300X the library. Selective
754 pressure via SINV infection (MOI 0,1) was applied to induce cell death (in red). DNA libraries
755 from input cells and cells surviving the dsRNA treatment as three independent biological
756 replicates were sequenced on an Illumina HiSeq4000. Comparison of the relative sgRNA
757 boundance in the Input and dsRNA condition were done using the MAGeCK standard pipeline
758 **B.** Median normalized read count distribution of all sgRNAs for the Input (in black) and SINV
759 (in red) replicates**. C.** Bubble plot of the candidate genes. Significance of RRA score was
760 calculated for each gene in the dsRNA condition compared to INPUT using the MAGeCK
761 software. The number of enriched sgRNAs for each gene is represented by the bubble size. The
762 gene ontology pathways associated to the significant top hits are indicated in orange and green.
763 **D.** Viability of cells upon SINV infection. Cells were infected with SINV at MOI of 0.1 then
764 the viability of the cells was quantified 24, 48 and 72 h post infection using PrestoBlue reagent.
765 One-way ANOVA analysis, * $p < 0.05$. **D.** SINV-GFP plaque assay. WT, COG4KO and
766 rescued HEK293T cells were infected with SINV-GFP for 24 and 48h at MOI of 1 and
767 supernatant was collected in order to measure viral production. The fold change in titer relative
768 to HEK293T arbitrarily set to 1 is shown. Average of three independent biological experiments
769 +/- SD is shown. Paired t.test analysis * $p < 0.05$.

770

771

772 **Supplemental information**

773

774 **Supplemental figures legends**

775 **Figure S1. Set up of the HCT116 cells as model for SINV infection and dsRNA-induced**
776 **cell death.**

777 **A.** Representative pictures of HCT116cas9 cells uninfected or infected with SINV-GFP MOI
778 of 1 at 24 and 48h post infection (hpi). 5X optical microscopy**. B.** Representative pictures of
779 HCT116cas9 cells at 24 and 48h post dsRNA (80 000 cells; 1 μg/mL) compared to non
780 transfected ones. 5X optical microscopy. **C.** Western blot of FLAG-Cas9 expression in
781 HCT116cas9 cells. Antibody against FLAG and GAPDH (normalizer) were used. **D-E**.
782 Distribution of sgRNA normalized read counts of selected genes. The read counts for the four
783 individual sgRNAs targeting enriched (*SLC35B2, BGAL4T7, COG4*) and not enriched genes
784 (*DDX58*, negative control) in the dsRNA samples (**D**) and in the SINV samples (**E**) over the
785 Input are shown.

786

787 **Figure S2. Generation of SLC35B2 and B4GALT7 HCT116 CRISPR/Cas9 knock-out**
788 **monoclonal cell lines.**

789 **A.** PCR screen of *SLC35B2* and *B4GALT7* knock-out clones obtained by CRISPR/Cas9. The
790 gels show the amplicons corresponding to wild type and deleted alleles that were subsequently
791 sequenced. **B.** Clustal Omega (48) alignment of the wild type and mutated peptide sequences
792 corresponding to the genomic deletions identified in the different clones. The reference
793 aminoacidic sequence is represented in yellow (unknown domains - InterPro) and orange
794 (known domains – InterPro). The peptidic sequences resulting in shorter protein due to
795 deletions or formation of premature stop codon in the knock-out clones are represented with
796 black bars or red rectangles, respectively.

797

798 **Figure S3**: **GFP plasmid transfectability in SLC35B2 and B4GALT7 HCT116**
799 **CRISPR/Cas9 KO cells.**

800 **A.** Representative pictures of GFP plasmid transfectability assay. Cells were transfected
801 (80 000 cells; 2 μg/mL) or nucleofected (200 000 cells; 500 ng) with a plasmid coding for GFP
802 and the GFP positive cells were observed by fluorescence microscopy at 24h (nucleofection)
803 or 48h (transfection) post treatment. Pictures were taken at 10× magnification, scale bar
804 represents 50 μm. **B.** GFP transfectability by FACS analysis. The different cell types were
805 transfected (80 000 cells; 2 μg/mL) with plasmid coding for GFP for 48h. The percentage of
806 GFP+ cells were determined by FACS analysis using a FACSCalibur. **C-D-E.** DNA plasmid
807 transfectability assay upon heparan-sulfates depletion. Cells were treated with 50 mM sodium
808 chlorate or with 2 units of heparinase then transfected with GFP plasmid. The relative number
809 of GFP positive (GFP+) cells (**C**), the GFP intensity of fluorescence (**D**) and the relative median
810 intensity of fluorescence of extracellular heparan-sulfates (HS) staining (**E**) were quantified
811 48h post transfection using FACS (10 000 events). Data from at least three independent
812 biological experiments +/- SD are shown. Paired t.test analysis, * $p < 0.05$.

813

814 **Figure S4. Characterization of the survival phenotype in HCT116 KO COG4 and**
815 **HEK293 KO COG4 cells.**

816 **A.** Viability assay. HCT116cas9 and HCT116cas9 KO COG4 cells (80 000 cells; 1 μg/mL)
817 were transfected with dsRNA then the cell viability was quantified 48 h post transfection using
818 PrestoBlue reagent. Data from at least three independent biological experiments are shown.
819 Paired t.test analysis, * $p < 0.05$. **B-C.** Cy5-labeled dsRNA transfection (80 000 cells; 1 μg/mL)
820 in HCT116cas9 and HCT116cas9 KO COG4 cells. Cy5 fluorescence was quantified using
821 FACSCalibur (10 000 events). The relative number of Cy5+ cells (**B**) and the relative median
822 of Cy5 intensity of fluorescence (**C**) compared to parental HCT116cas9 cells is shown. Average

823 of three experiments +/- SD are shown. Paired t.test analysis, * $p < 0.05$. **D.** Quantification of
824 extracellular heparan-sulfates. Upper panel correspond to FACS analysis of HEK293T control
825 (WT & rescued – respectively in red and orange) or HEK293T KO *COG4* (in blue) cells stained
826 with the HS-specific antibody 10E4 and lower panel show the unstained sample and HEK293T
827 KO *COG4*. One representative experiment out of three is shown. (10 000 events) **E-F.** GFP
828 transfectability by FACS analysis. HEK293T and HEK293T KO *COG4* cells were transfected
829 (80 000 cells; 2 μg/mL) with plasmid coding for GFP for 48h. The percentage of GFP+ cells
830 (**E**) and the relative median of GFP intensity of fluorescence (**F**) compared to parental
831 HEK293T cells was determined by FACS analysis using a FACSCalibur. Average of three
832 experiments +/- SD are shown Paired t.test analysis, * $p < 0.05$.
833
834 **Figure S5. Accumulation of GFP and dsRNA upon SINV infection in presence or absence**
835 **of COG4. A.** Representative pictures of HEK293T and HEK293T KO COG4 cells infected
836 with SINV-GFP MOI of 0.1 at 24 and 48h post infection (hpi). Pictures were taken at 20x
837 magnification. One representative experiment out of three is shown. **B.** DsRNA
838 immunofluorescence assay. Cells were infected with SINV at MOI of 0.1 for 24 h, then fixed
839 and stained with J2 antibody which recognizes dsRNA longer than 40bp and DAPI to stain the
840 nuclei. Pictures were taken at 40× magnification with BX51 (Olympus) microscope.
841
842 **Table S1**
843 List of primers used in the study.
844 **Dataset S1**
845 Count of sequenced sgRNA per genes in every replicates
846 **Dataset S2**
847 MAGeCK comparison report enriched sgRNAs in dsRNA versus Input samples

848 **Dataset S3**

849 MAGeCK comparison report enriched sgRNAs in SINV versus Input samples

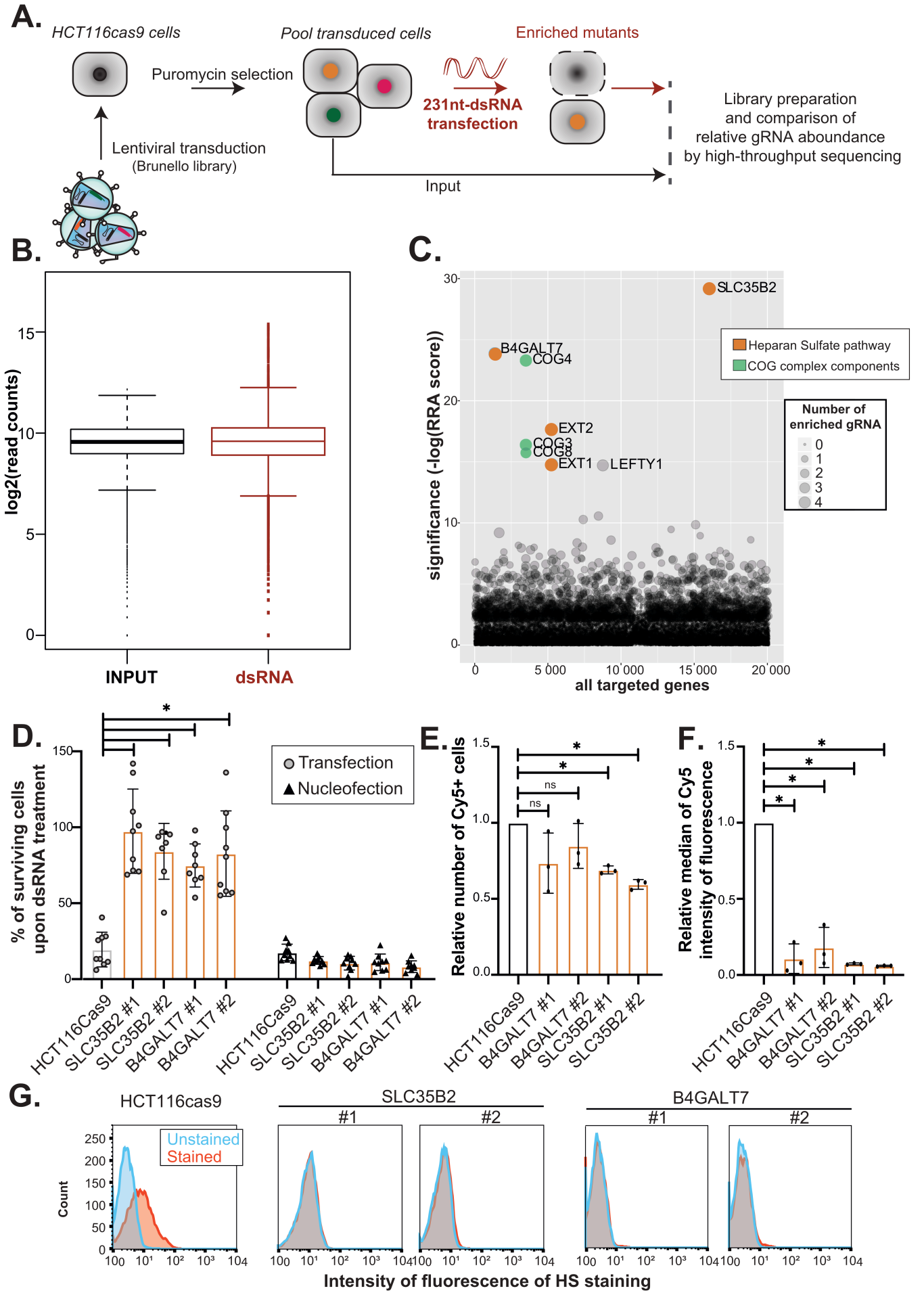
A.
HCT116cas9 cells
Puromycin selection
Pool transduced cells
Enriched mutants
231nt-dsRNA transfection
Library preparation and comparison of relative gRNA aboundance by high-throughput sequencing
Lentiviral transduction (Brunello library)
Input
B.
log2(read counts)
INPUT
dsRNA
C.
significance (-log(RRA score))
all targeted genes
SLC35B2
B4GALT7
COG4
EXT2
COG3
COG8
EXT1
LEFTY1
Heparan Sulfate pathway
COG complex components
Number of enriched gRNA
D.
% of surviving cells upon dsRNA treatment
Transfection
Nucleofection
HCT116Cas9
SLC35B2 #1
SLC35B2 #2
B4GALT7 #1
B4GALT7 #2
E.
Relative number of Cy5+ cells
ns
F.
Relative median of Cy5 intensity of fluorescence
G.
HCT116cas9
SLC35B2
B4GALT7
Unstained
Stained
Count
Intensity of fluorescence of HS staining

Figure 1

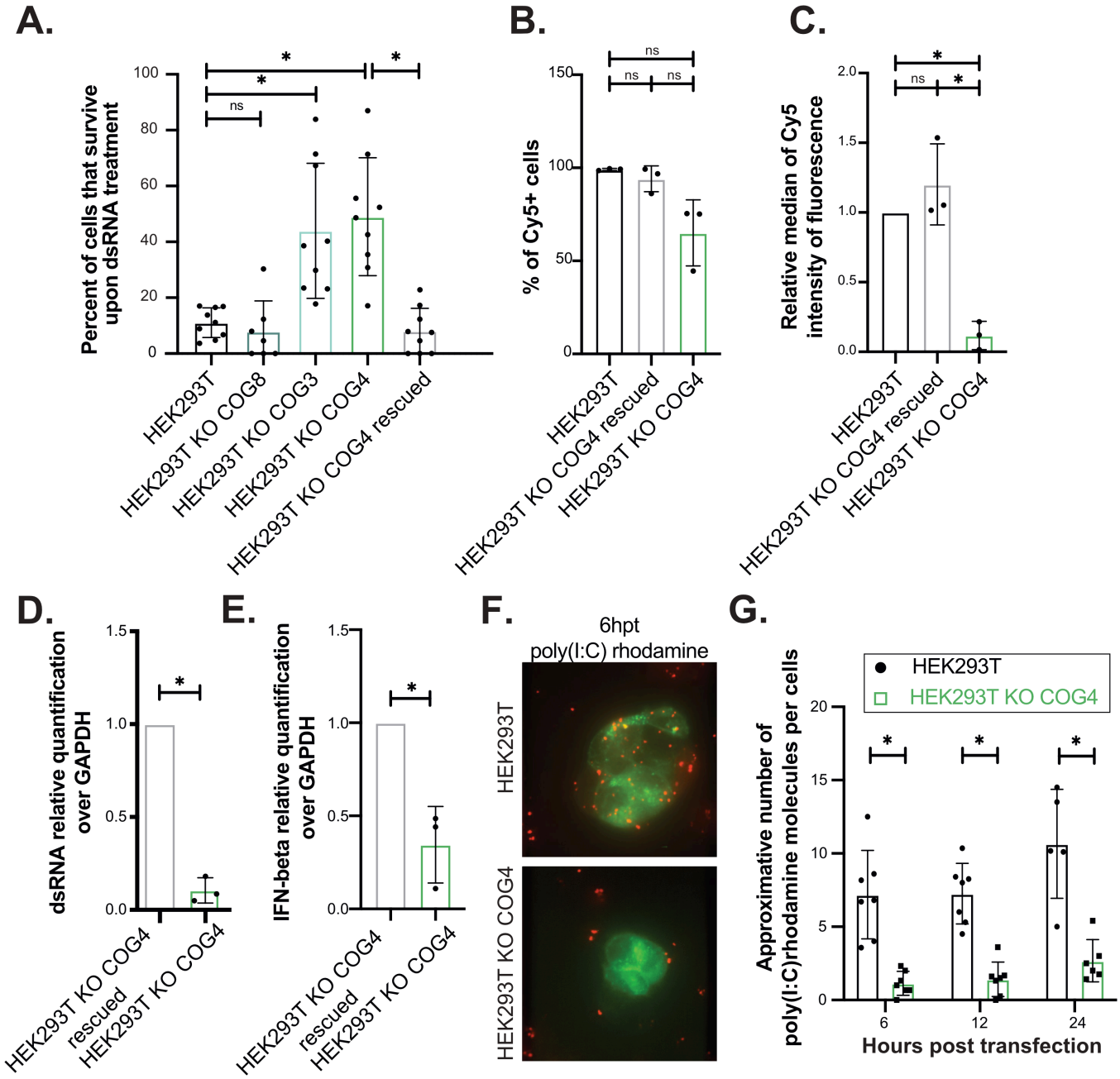
A.
Percent of cells that survive upon dsRNA treatment
100
80
60
40
20
0
*
*
*
ns
HEK293T
HEK293T KO COG8
HEK293T KO COG3
HEK293T KO COG4
HEK293T KO COG4 rescued
B.
% of Cy5+ cells
150
100
50
0
ns
ns
ns
HEK293T
HEK293T KO COG4 rescued
HEK293T KO COG4
C.
Relative median of Cy5 intensity of fluorescence
2.0
1.5
1.0
0.5
0.0
*
ns
*
HEK293T
HEK293T KO COG4 rescued
HEK293T KO COG4
D.
dsRNA relative quantification over GAPDH
1.5
1.0
0.5
0.0
*
HEK293T KO COG4 rescued
HEK293T KO COG4
E.
IFN-beta relative quantification over GAPDH
1.5
1.0
0.5
0.0
*
HEK293T KO COG4 rescued
HEK293T KO COG4
F.
6hpt
poly(I:C) rhodamine
HEK293T
HEK293T KO COG4
G.
HEK293T
HEK293T KO COG4
Approximative number of poly(I:C)rhodamine molecules per cells
20
15
10
5
0
*
*
*
6
12
24
Hours post transfection

Figure 2

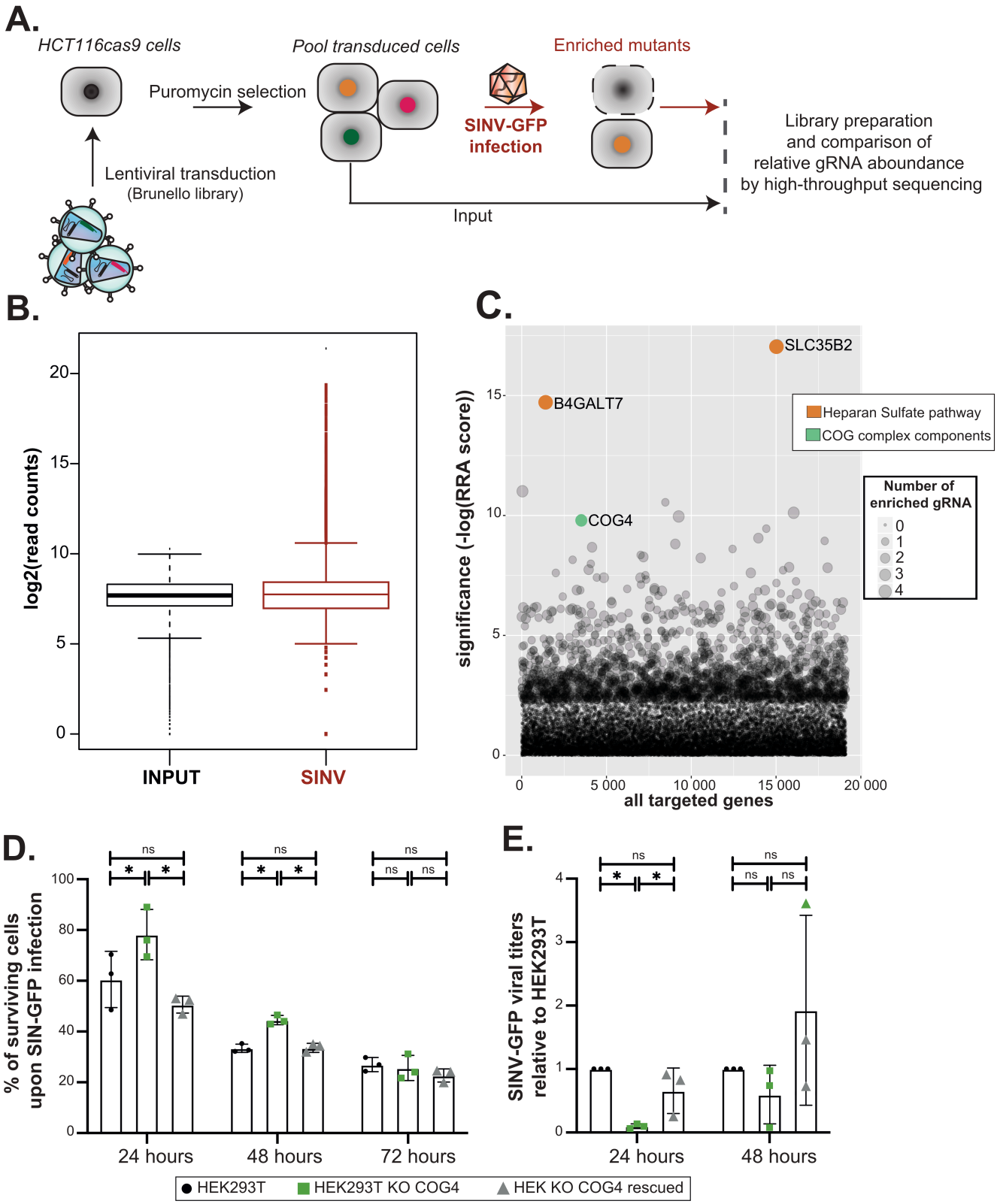
A.
HCT116cas9 cells
Puromycin selection
Pool transduced cells
Enriched mutants
SINV-GFP infection
Lentiviral transduction (Brunello library)
Input
Library preparation and comparison of relative gRNA aboundance by high-throughput sequencing
B.
log2(read counts)
INPUT
SINV
C.
SLC35B2
B4GALT7
COG4
Heparan Sulfate pathway
COG complex components
Number of enriched gRNA
significance (-log(RRA score))
all targeted genes
D.
% of surviving cells upon SIN-GFP infection
24 hours
48 hours
72 hours
E.
SINV-GFP viral titers relative to HEK293T
24 hours
48 hours
HEK293T
HEK293T KO COG4
HEK KO COG4 rescued

Figure 3

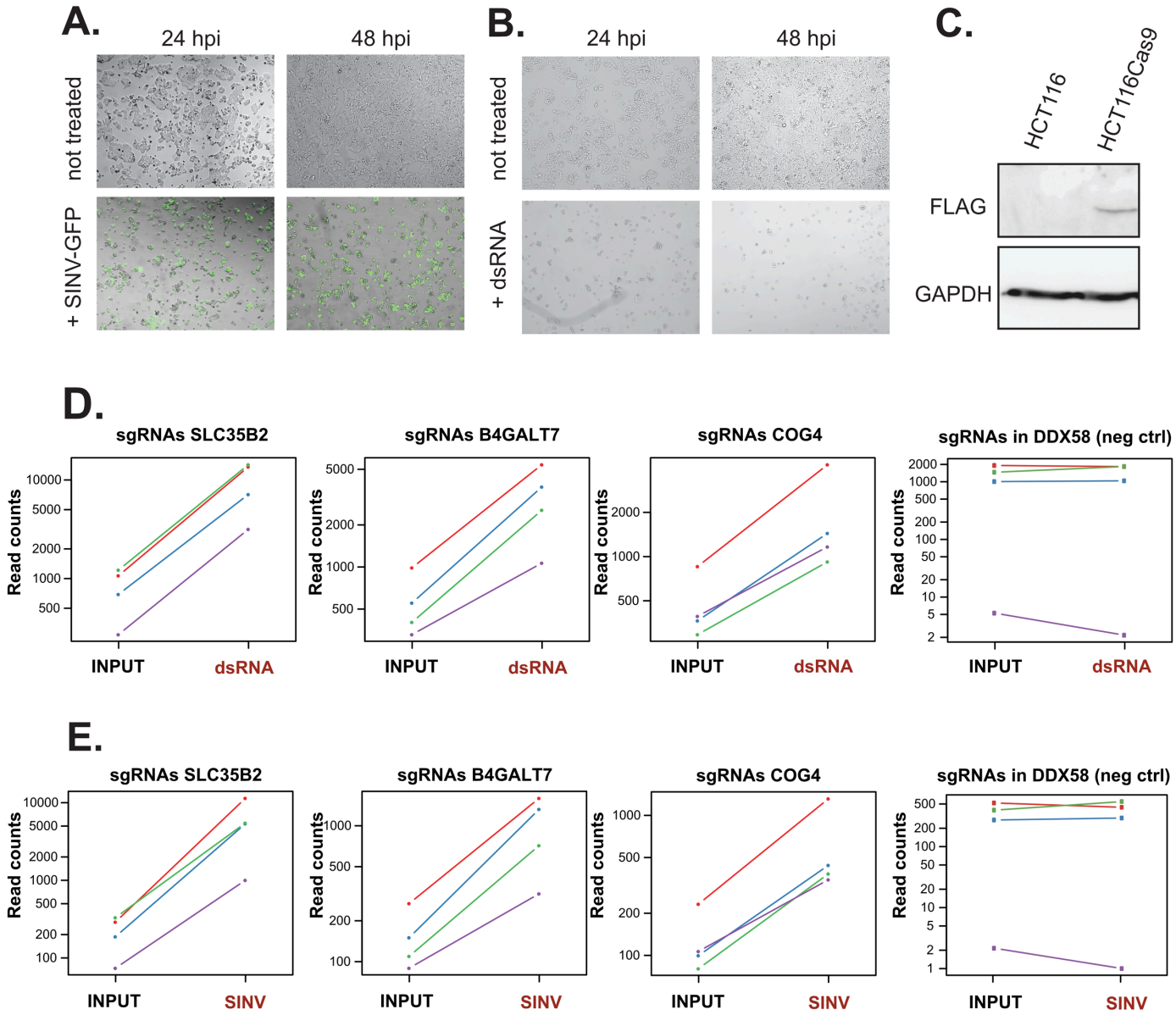
A.
24 hpi
48 hpi
not treated
+ SINV-GFP
B.
24 hpi
48 hpi
not treated
+ dsRNA
C.
HCT116
HCT116Cas9
FLAG
GAPDH
D.
sgRNAs SLC35B2
sgRNAs B4GALT7
sgRNAs COG4
sgRNAs in DDX58 (neg ctrl)
Read counts
INPUT
dsRNA
E.
sgRNAs SLC35B2
sgRNAs B4GALT7
sgRNAs COG4
sgRNAs in DDX58 (neg ctrl)
Read counts
INPUT
SINV

Figure S1

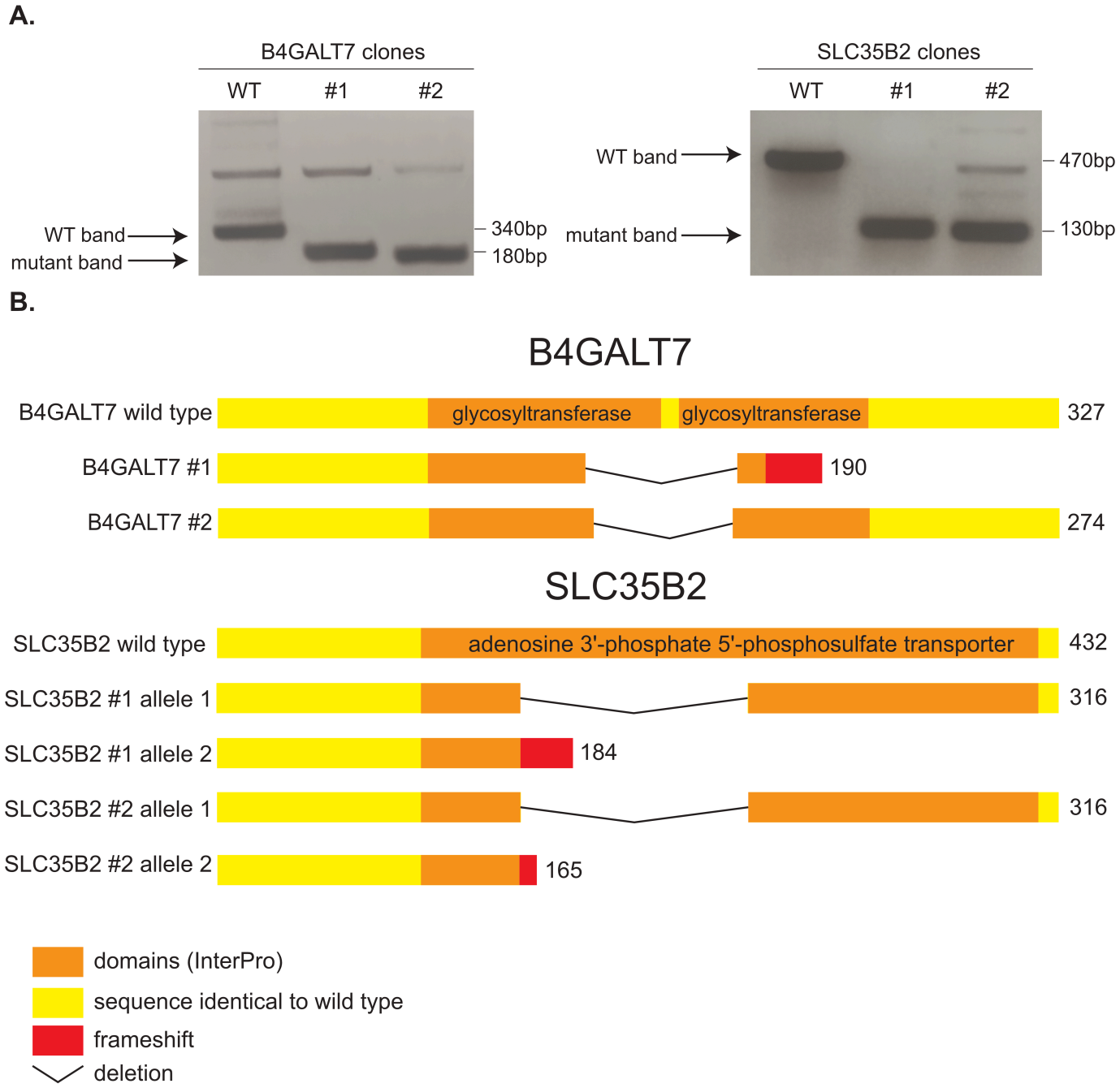
A.
B4GALT7 clones
WT
#1
#2
WT band
mutant band
340bp
180bp
SLC35B2 clones
WT
#1
#2
WT band
mutant band
470bp
130bp
B.
B4GALT7
B4GALT7 wild type
glycosyltransferase
glycosyltransferase
327
B4GALT7 #1
190
B4GALT7 #2
274
SLC35B2
SLC35B2 wild type
adenosine 3'-phosphate 5'-phosphosulfate transporter
432
SLC35B2 #1 allele 1
316
SLC35B2 #1 allele 2
184
SLC35B2 #2 allele 1
316
SLC35B2 #2 allele 2
165
domains (InterPro)
sequence identical to wild type
frameshift
deletion

Figure S2

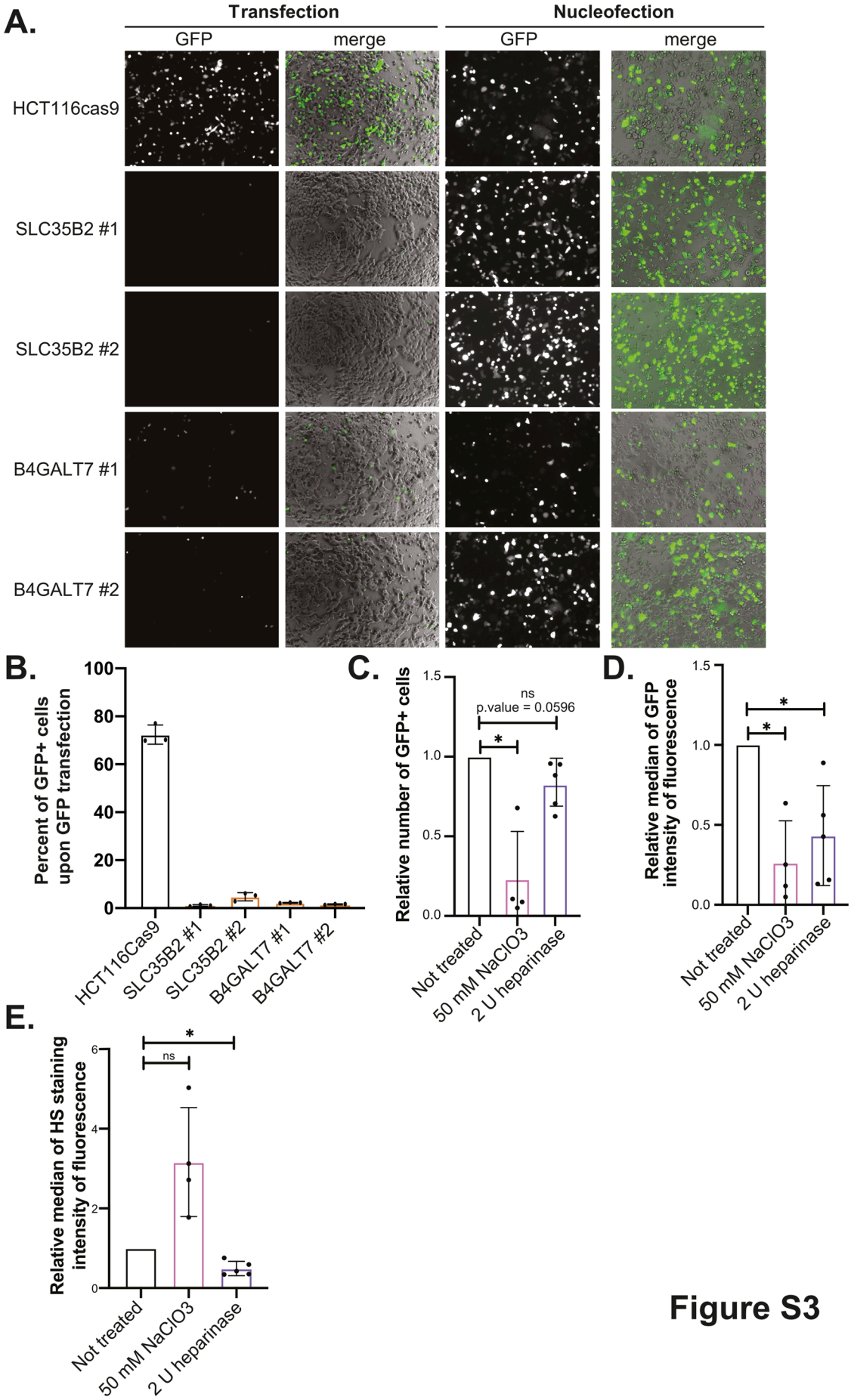
A.
Transfection
Nucleofection
GFP
merge
GFP
merge
HCT116cas9
SLC35B2 #1
SLC35B2 #2
B4GALT7 #1
B4GALT7 #2
B.
Percent of GFP+ cells upon GFP transfection
100
80
60
40
20
0
HCT116Cas9
SLC35B2 #1
SLC35B2 #2
B4GALT7 #1
B4GALT7 #2
C.
Relative number of GFP+ cells
1.5
1.0
0.5
0.0
ns
p.value = 0.0596
*
Not treated
50 mM NaClO3
2 U heparinase
D.
Relative median of GFP intensity of fluorescence
1.5
1.0
0.5
0.0
*
*
Not treated
50 mM NaClO3
2 U heparinase
E.
Relative median of HS staining intensity of fluorescence
6
4
2
0
*
ns
Not treated
50 mM NaClO3
2 U heparinase

Figure S3

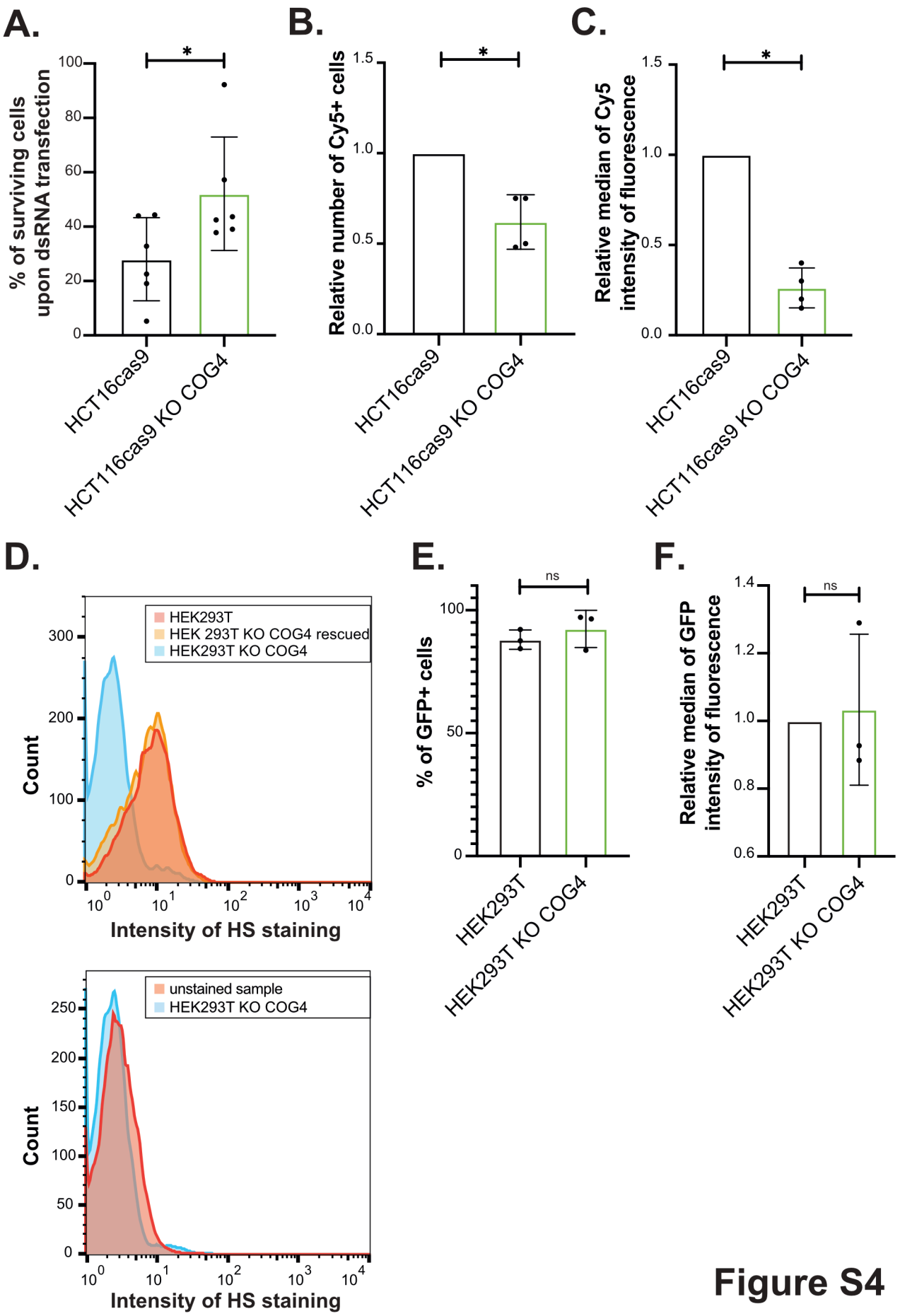
A.
% of surviving cells upon dsRNA transfection
100
80
60
40
20
0
*
HCT16cas9
HCT116cas9 KO COG4
B.
Relative number of Cy5+ cells
1.5
1.0
0.5
0.0
*
HCT16cas9
HCT116cas9 KO COG4
C.
Relative median of Cy5 intensity of fluorescence
1.5
1.0
0.5
0.0
*
HCT16cas9
HCT116cas9 KO COG4
D.
HEK293T
HEK 293T KO COG4 rescued
HEK293T KO COG4
Count
300
200
100
0
10^0 10^1 10^2 10^3 10^4
Intensity of HS staining
unstained sample
HEK293T KO COG4
Count
250
200
150
100
50
0
10^0 10^1 10^2 10^3 10^4
Intensity of HS staining
E.
% of GFP+ cells
100
50
0
ns
HEK293T
HEK293T KO COG4
F.
Relative median of GFP intensity of fluorescence
1.4
1.2
1.0
0.8
0.6
ns
HEK293T
HEK293T KO COG4

Figure S4

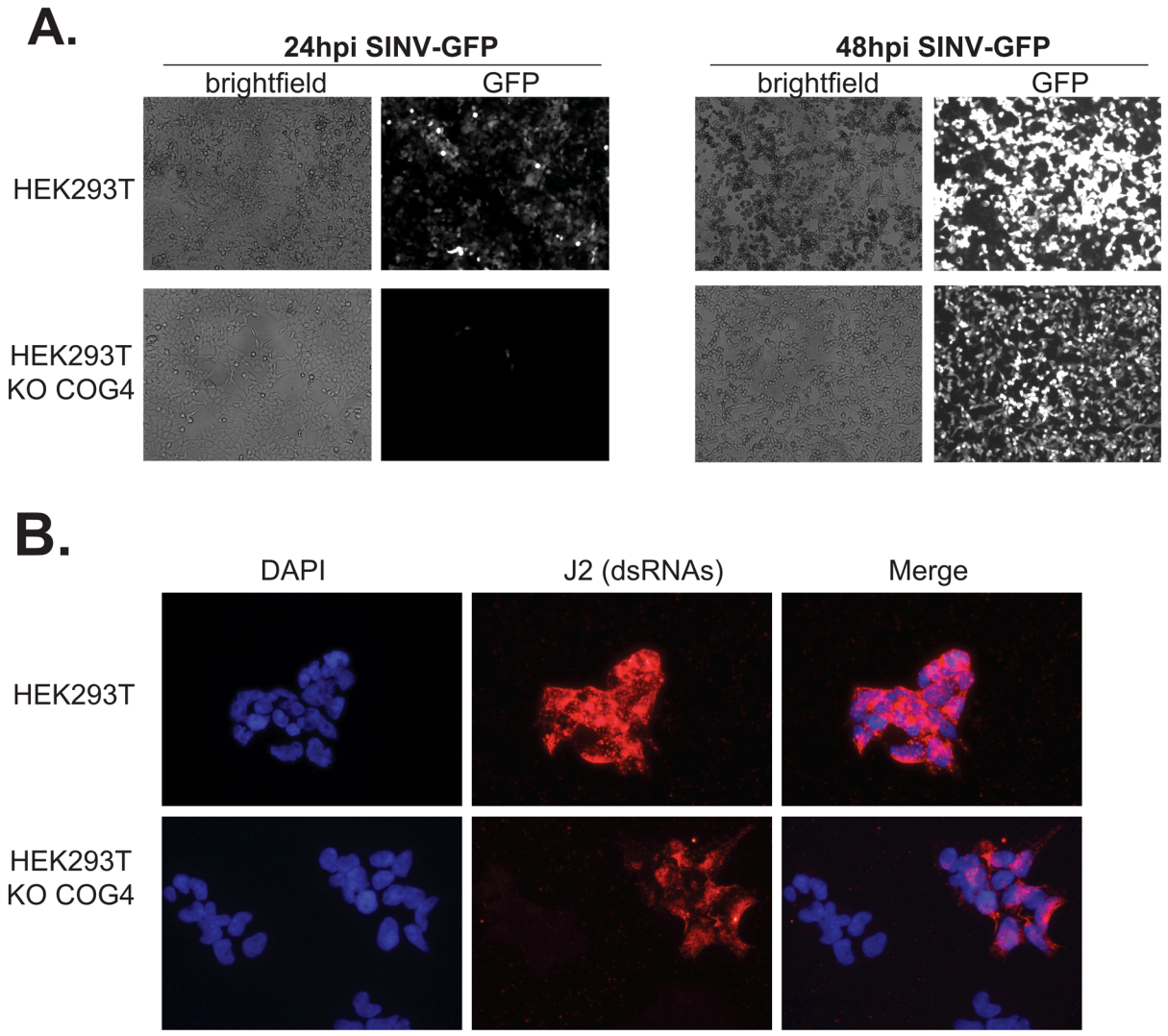
A.
24hpi SINV-GFP
48hpi SINV-GFP
brightfield
GFP
brightfield
GFP
HEK293T
HEK293T
KO COG4
B.
DAPI
J2 (dsRNAs)
Merge
HEK293T
HEK293T
KO COG4

Figure S5